

Revisiting Essential and Nonessential Settings of Evidential Deep Learning

Mengyuan Chen, Junyu Gao, and Changsheng Xu, *Fellow, IEEE*

Abstract—Evidential Deep Learning (EDL) is an emerging method for uncertainty estimation that provides reliable predictive uncertainty in a single forward pass, attracting significant attention. Grounded in subjective logic, EDL derives Dirichlet concentration parameters from neural networks to construct a Dirichlet probability density function (PDF), modeling the distribution of class probabilities. Despite its success, EDL incorporates several nonessential settings: In model construction, (1) a commonly ignored prior weight parameter is fixed to the number of classes, while its value actually impacts the balance between the proportion of evidence and its magnitude in deriving predictive scores. In model optimization, (2) the empirical risk features a variance-minimizing optimization term that biases the PDF towards a Dirac delta function, potentially exacerbating overconfidence. (3) Additionally, the structural risk typically includes a KL-divergence-minimizing regularization, whose optimization direction extends beyond the intended purpose and contradicts common sense, diminishing the information carried by the evidence magnitude. Therefore, we propose Re-EDL, a simplified yet more effective variant of EDL, by relaxing the nonessential settings and retaining the essential one, namely, the adoption of projected probability from subjective logic. Specifically, Re-EDL treats the prior weight as an adjustable hyperparameter rather than a fixed scalar, and directly optimizes the expectation of the Dirichlet PDF provided by deprecating both the variance-minimizing optimization term and the divergence regularization term. Extensive experiments and state-of-the-art performance validate the effectiveness of our method. The source code is available at <https://github.com/MengyuanChen21/Re-EDL>.

Index Terms—Uncertainty quantification, Evidential Deep Learning, Subjective Logic Theory.

arXiv:2410.00393v1 [cs.LG] 1 Oct 2024

1 INTRODUCTION

IN high-risk domains such as autonomous driving and medical analysis, it is imperative for models to reliably convey the confidence or uncertainty level of their predictions [1], [2]. Despite effective uncertainty quantification methods based on Bayesian theory and ensemble techniques have been developed, these mainstream methods necessitate multiple forward passes in the inference phase [3]–[8], imposing substantial computational burdens that hamper their widespread industrial adoption. This limitation drives the interest of researchers in exploring how to achieve high-quality uncertainty estimation with minimal additional cost.

Evidential deep learning (EDL) [9] is such a newly arising single-forward-pass uncertainty estimation method, which has attracted increasing attention for its success in various pattern recognition tasks [10]–[18]. Drawing upon the subjective logic theory [19], [20], EDL employs deep neural networks to derive Dirichlet concentration parameters, constructing a Dirichlet distribution that models the distribution of class probabilities and enables high-quality uncertainty estimation. Specifically, in C -class classification, EDL models the distribution of class probability \mathbf{p}_X with a constructed Dirichlet distribution $\text{Dir}(\mathbf{p}_X, \boldsymbol{\alpha}_X)$, whose concentration parameter vector $\boldsymbol{\alpha}_X(x)$ is given by

$$\boldsymbol{\alpha}_X(x) = \mathbf{e}_X(x) + C \cdot \mathbf{a}_X(x), \quad \forall x \in \mathbb{X} = \{1, 2, \dots, C\}, \quad (1)$$

- Mengyuan Chen, Junyu Gao and Changsheng Xu are with National Lab of Pattern Recognition, Institute of Automation, Chinese Academy of Sciences, Beijing 100190, P. R. China, and with University of Chinese Academy of Sciences, Beijing, China, and also with Peng Cheng Laboratory, ShenZhen, China (e-mail: chenmengyuan2021@ia.ac.cn; junyu.gao@nlpr.ia.ac.cn; csxu@nlpr.ia.ac.cn).

Manuscript received April 19, 2021; revised August 16, 2021.

where the base rate \mathbf{a}_X is typically set as a uniform distribution over \mathbb{X} , and its scalar coefficient C serves as a parameter termed as a *prior weight*. Note that to keep the notation uncluttered, we use $\boldsymbol{\alpha}_X(x)$ as a simplified expression of $\boldsymbol{\alpha}_X(X = x)$, and similarly for $\mathbf{e}_X(x)$ and $\mathbf{a}_X(x)$. The random variable X denotes the class index of the input sample, and $\mathbf{e}_X(x)$ signifies the amassed evidence for the sample's association with class x . Thereafter, for model optimization, the traditional EDL method integrates the mean square error (MSE) loss over the class probability \mathbf{p}_X , which is assumed to follow the above Dirichlet distribution, thus deriving the empirical risk (average loss over training samples) as

$$\begin{aligned} \mathcal{L}_{\text{edl-emp}} &= \frac{1}{|\mathcal{D}|} \sum_{(\mathbf{z}, \mathbf{y}) \in \mathcal{D}} \mathbb{E}_{\mathbf{p}_X \sim \text{Dir}(\mathbf{p}_X, \boldsymbol{\alpha}_X)} [\|\mathbf{y} - \mathbf{p}_X\|_2^2] \\ &= \frac{1}{|\mathcal{D}|} \sum_{(\mathbf{z}, \mathbf{y}) \in \mathcal{D}} \sum_{x \in \mathbb{X}} (\mathbf{y}_x - \mathbb{E}_{\mathbf{p}_X \sim \text{Dir}(\mathbf{p}_X, \boldsymbol{\alpha}_X)}[\mathbf{p}_X(x)])^2 \quad (2) \\ &\quad + \text{Var}_{\mathbf{p}_X \sim \text{Dir}(\mathbf{p}_X, \boldsymbol{\alpha}_X)}[\mathbf{p}_X(x)], \end{aligned}$$

where the training set \mathcal{D} consists of sample features and their one-hot labels denoted $(\mathbf{z}, \mathbf{y})^1$, and \mathbf{y}_x refers to the x -th element of \mathbf{y} . In addition, the structural risk (loss with extra regularization to mitigate over-fitting) of EDL-related methods typically include an additional regularization \mathcal{L}_{kl} ,

$$\mathcal{L}_{\text{kl}} = \frac{1}{|\mathcal{D}|} \sum_{(\mathbf{z}, \mathbf{y}) \in \mathcal{D}} \text{KL}(\text{Dir}(\mathbf{p}_X, \tilde{\boldsymbol{\alpha}}_X), \text{Dir}(\mathbf{p}_X, \mathbf{1})), \quad (3)$$

where $\mathbf{1}$ denotes a C -dimensional ones vector, and $\tilde{\boldsymbol{\alpha}}_X = \mathbf{y} + (\mathbf{1} - \mathbf{y}) \odot \boldsymbol{\alpha}_X$ represents a modified Dirichlet parameter

1. In deep learning, the sample feature is usually denoted by \mathbf{x} . However, to preclude ambiguity with x as the value of the random variable X , we employ \mathbf{z} instead to denote the sample feature. Random variable X , label \mathbf{y} , and feature \mathbf{z} all pertain to the same input sample.

vector where the target class value is set to 1. \mathcal{L}_{kl} expects to minimize the Kullback-Leibler divergence between a uniform distribution and a modified Dirichlet distribution (hereafter referred to as *KL-Div-minimizing* for short), thereby suppressing evidence of non-target categories.

Despite the remarkable success of EDL, we argue that the existing EDL-based methods incorporate nonessential settings in both model construction and model optimization. These settings have been widely accepted by deep learning researchers; however, they are not intrinsically mandated by the mathematical framework of subjective logic and, based on our research, have minimal impact on enhancing uncertainty estimation in most cases. Specifically, in model construction, (1) the commonly ignored prior weight parameter in Eqn. 1 governs the balance between capitalizing on the proportion of evidence and its magnitude when deriving predictive scores. However, EDL prescribes this parameter’s value to be equivalent to the number of classes, potentially resulting in highly counter-intuitive outcomes. Therefore, we advocate for setting the prior weight parameter as a free hyperparameter in the neural network to adapt to complex application cases. In model optimization, (2) the empirical risk given by Eqn. 2 includes a variance-minimizing optimization term, which encourages the Dirichlet PDF modeling the distribution of probabilities to approach a Dirac delta function which is infinitely high and infinitesimally thin, or in other words, requires an infinite amount of evidence of the target class, thus further intensifying the over-confidence issue. (3) When designing the structural risk, EDL-related works commonly incorporate a KL-Div-minimizing regularization term \mathcal{L}_{kl} , as formulated in Eqn. 3. Our analysis suggests that its optimization direction extends beyond the intended purpose and contradicts common sense, diminishing the information carried by evidence magnitude. Therefore, we advocate for directly optimizing the expectation of the Dirichlet distribution towards one-hot labels, deprecating both the variance-minimizing optimization term and the KL-divergence regularization to obtain more reliable predictive scores. Note that our relaxations strictly adhere to the subjective logic theory.

Relaxing the nonessential EDL settings that are not mandated by subjective logic and often bring minimal benefit, we naturally become curious about the truly essential setting that contributes to the uncertainty estimation capability of EDL. In this work, we identify the adoption of projected probability from subjective logic as the essential setting. Specifically, compared to the traditional softmax operation, projected probability introduces an extra parameter to class scores and utilizes an output activation function characterized by a more gradual growth rate than the Exp function, both of which lead to more effective preservation of the magnitude information carried by model output logits.

In summary, as presented in Fig. 1, we develop a simplified yet more effective EDL variant by deprecating the nonessential settings while retaining the essential ones. To distinguish it from R-EDL [21], the conference version which also relaxes EDL settings, we refer to the method introduced in this work as **Re-EDL**. This name highlights its derivation from **Revisiting** EDL settings, while also indicating its relevance to the earlier R-EDL. Our contributions include:

- An analysis of the commonly ignored prior weight

parameter which balances the trade-off relationship between leveraging the proportion and magnitude of evidence in the subjective logic framework.

- An analysis of the benefits of directly applying the MSE loss to the expected value of the constructed Dirichlet distribution as the empirical risk, rather than integrating the MSE loss over the class probabilities p_X drawn from this Dirichlet distribution.
- An analysis of the optimization direction and practical impact of the KL-Div-minimizing regularization, which is commonly adopted in EDL’s structural risk but considered by us as nonessential since it often hinders uncertainty quantification by causing information loss in evidence amplitude.
- An exploration of the truly essential setting in EDL, namely, the adoption of projected probability from subjective logic theory, which contributes to the superior uncertainty estimation capability within the context of our simple Re-EDL formulation.
- Experiments on multiple benchmarks for uncertainty estimation, which comprehensively demonstrate the effectiveness of our proposed method under the classical, few-shot, video-modality, and noisy settings.

A preliminary version of this work [21] has been accepted for a Spotlight presentation at ICLR 2024. In this paper, we extend our previous work both theoretically and empirically. **Theoretically**, (1) we analyze that the commonly adopted KL-Div-minimizing regularization is a nonessential EDL setting, since its optimization extends beyond the intended purpose and contradicts common sense, typically causing information loss in evidence amplitude and hindering uncertainty estimation. (2) Additionally, we analyze that replacing traditional softmax classification head with projected probability is a truly essential EDL setting which contributes to the superior uncertainty estimation, since the components of projected probability better preserve the amplitude information of model logits. (3) Therefore, we propose Re-EDL by relaxing the nonessential EDL settings and retaining only the essential one, which achieves impressive simplicity and uncertainty estimation capability. **Empirically**, (4) we highlight a series of in-depth experiments which support our arguments regarding the essential and nonessential EDL settings. (5) Furthermore, we include more recent baseline methods and expand the original experimental setup from [21] by including four additional OOD datasets to ensure a comprehensive evaluation. Key baseline methods are reproduced under consistent training settings, enhancing the fairness of comparisons. Additional introductions, ablations, and visualizations are provided.

Due to space limitations, derivations, proofs, additional introductions, and extra results are provided in Appendix.

2 RELATED WORK

Theoretical Extensions of EDL. A comprehensive introduction to EDL [9] is provided in Section 3.2. Here, we offer a brief overview of the subsequent developments of EDL. Early research primarily focuses on enhancing the model’s uncertainty estimation capabilities by incorporating additional OOD samples. For instance, [22] employs generative models to obtain proximal OOD samples, using

the latent space of a variational autoencoder (VAE) [23] as a proxy for semantic similarity. [24] extends this approach by leveraging both proximal and distant OOD samples to further improve uncertainty estimation. Besides, [25], [26] explores the use of pre-prepared OOD samples to enhance the performance of EDL models. Recent advancements in EDL classification theory have primarily focused on exploring alternative methods for evidence collection. For instance, [27] introduces an innovative evidence collection paradigm that gathers evidence from multiple intermediate layers, rather than relying solely on the final network layer. RED [28] conducts a deep analysis of evidential activation functions and proposes a novel regularizer that effectively addresses existing limitations. \mathcal{I} -EDL, proposed by [29], incorporates the Fisher information matrix to assess the evidence informativeness carried by samples. Additionally, HENN [30] proposes a generalized variant of EDL, extending the multinomial subjective opinion characterized by EDL to a hypernomial version. Furthermore, [31] combines EDL, neural processes, and neural Turing machines to propose the Evidential Tuning Process, which shows stronger performances than EDL but requires a rather complex memory mechanism. Compared with previous efforts, our method is the first to revisit essential and nonessential EDL settings, leading to a simplified yet superior EDL variant.

Widespread Applications of EDL. EDL has been widely applied across various downstream application fields, including computer vision [11], [22], [24], [26], [32]–[42], natural language processing [43]–[45], cross-modal learning [12], [46]–[48], and other scientific subjects such as medicine [32], physics [49], chemistry [50], etc. From the perspective of machine learning paradigms, except for supervised learning, EDL has also achieved success within active learning [15], [16], [51], transfer learning [52]–[55], reinforcement learning [56], [57], weakly-supervised learning [42], [58], [59], few-shot learning [60], etc. Besides, Deep Evidential Regression (DER) [10], [61] successfully extends the application field of EDL to regression by incorporating evidential priors into the Gaussian likelihood function, thereby enhancing uncertainty modeling in regression networks. Moreover, [14], [62]–[68] also provides valuable explorations in DER.

Other single-model uncertainty methods based on DNNs. In addition to EDL-related works, various single-model methods exist for estimating predictive uncertainties. Efficient ensemble methods [4], [7], which cast a set of models under a single one, show state-of-the-art performances on large-scale datasets. While these methods are parameter-efficient, they necessitate multiple forward passes during inference. Bayesian Neural Networks (BNNs) [69], [70] model network parameters as random variables and quantify uncertainty through posterior estimation while suffering from a significant computational cost. A widely-recognized method is Monte Carlo Dropout [5], which interprets the dropout layer as a random variable following a Bernoulli distribution, and training a neural network with such dropout layers can be considered an approximation to variational inference. Two other notable single-forward-pass methods, DUQ [71] and SNGP [72], introduce distance-aware output layers using radial basis functions or Gaussian processes. Although nearly competitive with deep ensembles in OOD benchmarks, these methods entail extensive

modifications to the training procedure and lack easy integration with existing classifiers. Another group of efficient uncertainty methods are Dirichlet-based uncertainty (DBU) methods, to which EDL also belongs. Prominent DBU methods encompass KL-PN [73], RKL-PN [74], PostN [75], and NatPN [76], which vary in both the parameterization and the training strategy of the Dirichlet distribution. Compared to these preceding methods, our approach combines the benefits of exhibiting favorable performances, being single-forward-pass, parameter-efficient, and easily integrable.

Comparing Subjective Logic with other Uncertainty Reasoning Frameworks. Please refer to Appendix B.1.

3 PRELIMINARY: FROM SUBJECTIVE LOGIC TO EVIDENTIAL DEEP LEARNING

The essence of Evidential Deep Learning (EDL) lies in employing DNNs as analysts within the framework of subjective logic. In this section, we briefly introduce core concepts of subjective logic theory (Section 3.1), and outline the primary steps involved in developing EDL (Section 3.2). This introduction aims to differentiate between the fundamental theoretical requirements and the optional practical implementations, facilitating the subsequent discussion on the essential and nonessential settings of EDL (Section 4).

3.1 Subjective Logic Theory

Just as the names of *binary* logic and *probabilistic* logic imply, an argument in binary logic must be either true or false, and while probabilistic logic allows for probabilities within the range $[0, 1]$ to express partial true. However, both binary logic and probabilistic logic deal with definite arguments and do not provide a mechanism to express uncertainty or indifference, such as saying “*I don’t know*”. To address this limitation, subjective logic [19], [20] extends probabilistic logic by explicitly including uncertainty about probabilities in the formalism. Specifically, an argument in subjective logic, also called a *subjective opinion*, is formalized as follows:

Definition 1 (Subjective opinion). Given a categorical random variable X on the domain \mathbb{X} , a subjective opinion over X is defined as the ordered triplet $\omega_X = (\mathbf{b}_X, u_X, \mathbf{a}_X)$, where \mathbf{b}_X is a *belief mass* distribution over X , u_X is a *uncertainty mass*, \mathbf{a}_X is a *base rate*, aka a prior probability distribution over X , and the additivity requirements $\sum_{x \in \mathbb{X}} \mathbf{b}_X(x) + u_X = 1$ and $\sum_{x \in \mathbb{X}} \mathbf{a}_X(x) = 1$ are satisfied.

Belief mass $\mathbf{b}_X(x)$ assigned to a singleton value $x \in \mathbb{X}$ expresses support for the statement $X = x$ being TRUE, and uncertainty mass can be interpreted as belief mass assigned to the entire domain. Therefore, subjective logic also provides a well-defined *projected probability*, which follows the additivity requirement of traditional probability theory, by reassigning the uncertainty mass into each singleton of domain \mathbb{X} according to the base rate \mathbf{a}_X as follows:

Definition 2 (Projected probability). The projected probability P_X of the subjective opinion $\omega_X = (\mathbf{b}_X, u_X, \mathbf{a}_X)$ is defined by $P_X(x) = \mathbf{b}_X(x) + \mathbf{a}_X(x)u_X, \forall x \in \mathbb{X}$. Note that the additivity requirement $\sum_{x \in \mathbb{X}} P_X(x) = 1$ is satisfied.

Furthermore, the subjective logic theory points out that, if the base rate \mathbf{a}_X and a parameter termed prior weight, denoted as W , is given, there exists a bijection between a

multinomial opinion and a Dirichlet probabilistic density function (PDF) as presented in Theorem 1. This relationship emerges from interpreting second-order uncertainty by probability density, and plays an important role in the formalism of subjective logic since it provides a calculus reasoning with PDFs. The proof is provided in Appendix A.1.

Theorem 1 (Bijection between subjective opinions and Dirichlet PDFs). Consider a random variable X defined on the domain \mathbb{X} , and let $\omega_X = (\mathbf{b}_X, u_X, \mathbf{a}_X)$ represent a subjective opinion. Denote by \mathbf{p}_X a probability distribution over \mathbb{X} , and let the Dirichlet PDF with concentration parameter α_X be denoted as $\text{Dir}(\mathbf{p}_X, \alpha_X)$, where $\alpha_X(x) \geq 0$ and $\mathbf{p}_X(x) \neq 0$ when $\alpha_X(x) < 1$. Given the base rate \mathbf{a}_X , there exists a bijection F that maps the subjective opinion ω_X to the Dirichlet PDF $\text{Dir}(\mathbf{p}_X, \alpha_X)$ as follows:

$$F : \omega_X = (\mathbf{b}_X, u_X, \mathbf{a}_X) \mapsto \text{Dir}(\mathbf{p}_X, \alpha_X) = \frac{\Gamma(\sum_{x \in \mathbb{X}} \alpha_X(x))}{\prod_{x \in \mathbb{X}} \Gamma(\alpha_X(x))} \prod_{x \in \mathbb{X}} \mathbf{p}_X(x)^{\alpha_X(x)-1}, \quad (4)$$

where Γ denotes the Gamma function, and α_X satisfies that

$$\alpha_X(x) = \frac{\mathbf{b}_X(x)W}{u_X} + \mathbf{a}_X(x)W, \quad \forall x \in \mathbb{X}, \quad (5)$$

and $W \in \mathbb{R}_+$ is a scalar called a prior weight, whose setting will be further discussed in Section 4.1.

3.2 Evidential Deep Learning

Based on subjective logic, [9] proposes a single-forward-pass uncertainty estimation method named Evidential Deep Learning (EDL), which lets deep neural networks play the role of analysts to give belief mass and uncertainty mass of samples. For example, in C -class classification, the belief mass \mathbf{b}_X and uncertainty mass u_X of the input sample, whose category index is a random variable X taking values x from the domain $\mathbb{X} = [1, \dots, C]$, are given by

$$\mathbf{b}_X(x) = \frac{e_X(x)}{S_X}, \quad u_X = \frac{C}{S_X}, \quad S_X = \sum_{x \in \mathbb{X}} e_X(x) + C. \quad (6)$$

Specifically, $e_X(x)$, which denotes the *evidence* of the random variable X taking the value x , is the x -th element of the evidence vector $\mathbf{e}_X = f(g(\mathbf{z})) \in \mathbb{R}_+^C$, where \mathbf{z} is the feature of the input sample, g is a deep neural network, f is a non-negative output activation function (e.g., softplus), sometimes also called *evidence function*, and the scalar C in this equation serves as the prior weight.

According to Theorem 1, there exists a bijection between the Dirichlet PDF denoted $\text{Dir}_X(\mathbf{p}_X, \alpha_X)$ and the opinion $\omega_X = (\mathbf{b}_X, u_X, \mathbf{a}_X)$ if the requirement in Eqn. 5 is satisfied. Substituting Eqn. 6 into Eqn. 5 and setting the prior weight W in Eqn. 5 as C , we obtain the relationship between the parameter vector of the Dirichlet PDF and the collected evidence in EDL, as expressed by Eqn. 1. Moreover, since EDL sets the base rate $\mathbf{a}_X(x)$ as a uniform distribution, the relationship given by Eqn. 1 can be further simplified into $\alpha_X(x) = \mathbf{e}_X(x) + 1, \forall x \in \mathbb{X}$.

To perform model optimization, EDL integrates the MSE loss function over the class probability \mathbf{p}_X which is assumed to follow the Dirichlet PDF specified in the bijection, thus derives the empirical risk given by Eqn. 2. Moreover, the structural risk of EDL-related methods typically includes

a KL-Div-minimizing regularization, formulated in Eqn. 3, to suppress evidence of non-target categories. The detailed derivations are provided in Appendix A.2. In inference, EDL utilizes the projected probability \mathbf{P}_X (refer to Definition 2),

$$\mathbf{P}_X(x) = \mathbf{b}_X(x) + \mathbf{a}_X(x)u_X = \frac{e_X(x) + 1}{S_X} = \frac{\alpha_X(x)}{S_X}, \quad (7)$$

as the predictive scores, and uses Eqn. 6 to calculate the uncertainty mass u_X as the uncertainty of classification.

4 RE-EDL: REVISIT ESSENTIAL AND NONESSENTIAL SETTINGS OF EDL

Despite the significant success of EDL, we argue that the existing EDL-based methodologies (Section 3.2) retain several rigid settings, which, while widely accepted, are not intrinsically mandated within subjective logic (Section 3.1) and typically offer minimal benefit to uncertainty quantification. Specifically, in this section, we identify the following nonessential EDL settings: In model construction, **(1)** a **prior weight** parameter is fixed to the number of classes, suppressing the model's ability to adjust the impact of evidence magnitude and its proportion on predictions (Section 4.1); In model optimization, **(2)** for the **empirical risk** (average loss over training samples), traditional EDL adopts the expected value of the MSE loss over the constructed Dirichlet distribution rather than directly applying MSE to the expected value of the Dirichlet distribution. This results in an additional variance-minimizing term, which exacerbates overconfidence. (Section 4.2); **(3)** For the **structural risk** (loss with extra regularization terms), a commonly adopted KL-Div-minimizing regularization on non-target evidence limits model's complexity but hampers uncertainty estimation in most situations (Section 4.3). After relaxing the above nonessential EDL settings while strictly adhering to subjective logic, we further provide an in-depth discussion about the truly essential EDL settings which contribute to the superior uncertainty estimation capability (Section 4.4).

4.1 Relaxing the Rigid Setting of Fixing Prior Weight in Model Construction

In this subsection, we elucidate how the prior weight W balances between leveraging the proportion and magnitude of evidence to compute predictive scores. Conclusively, we argue against the rigidity of fixing W to the class number and propose viewing it as an adjustable hyperparameter.

The nomenclature of **prior weight** comes from the expression of Eqn. 1. The scalar coefficient C , functioning as the prior weight W , denotes the weight of the base rate \mathbf{a}_X , which is alternatively termed the **prior distribution**. In Theorem 1, it should be noted that the bijection between subjective opinions and Dirichlet PDFs is only specified when the base rate \mathbf{a}_X and the prior weight W are given. Typically, in the absence of prior information, we default to setting the base rate as a uniform distribution over the domain \mathbb{X} , i.e., $\mathbf{a}_X(x) = 1/|\mathbb{X}| = 1/C, \forall x \in \mathbb{X}$. However, the setting of the prior weight W is worth further discussion.

We argue that fixing the prior weight to the cardinality of the domain, which is widely adopted by EDL researchers, is not intrinsically mandated by subjective logic and may result in counter-intuitive results. For example, a

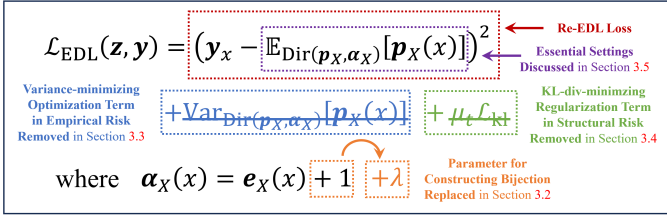


Fig. 1: A conceptual framework diagram illustrating the essential and nonessential settings discussed in Section 4. By relaxing the nonessential settings while retaining the essential ones, the proposed Re-EDL method achieves more superior uncertainty estimation with reduced complexity.

100-class classification task forces $W = 100$. Even though the neural net gives an extreme evidence distribution $e = [100, 0, 0, \dots, 0] \in \mathbb{R}_+^{100}$, EDL will reach the prediction that the probability of the sample belonging to Class 1 is $P = (100 + 1)/(100 + 100) \approx 0.5$ by Eqn. 7, which is highly counter-intuitive. The underlying reason is that the value of W dictates the degree to which the projected probability is influenced by the **magnitude** of the evidence or contrarily the **proportion** of the evidence. To elucidate this point more clearly, we first revisit Eqn. 6 and Eqn. 7 without fixing the prior weight W to C . In this way, we can obtain a generalized form of the projected probability P_X as

$$P_X(x) = b_X(x) + a_X(x)u_X = \frac{e_X(x) + \frac{W}{C}}{\sum_{x' \in \mathbb{X}} e_X(x') + W}. \quad (8)$$

When the prior weight W is set to zero, the projected probability P_X in Eqn. 8 degenerates to a conventional probability form, which solely relies on the proportion of evidence among classes and is unaffected by their magnitude, as scaling the evidence by a constant coefficient has no impact on P_X . However, when W is not zero, we have

$$P_X(x) \leq \frac{e_X(x) + \frac{W}{C}}{e_X(x) + W} = 1 - \left(1 - \frac{1}{C}\right) \cdot \frac{1}{e_X(x)/W + 1}, \quad (9)$$

where the equality holds only if $\sum_{x' \in \mathbb{X}, x' \neq x} e_X(x') = 0$. Eqn. 9 indicates that with extreme evidence distributions, where evidence for all classes except class x is zero, the upper bound of $P_X(x)$ is determined by the ratio of the evidence for class x to the prior weight W . In other words, given the prior weight W , the upper bound of $P_X(x)$ purely relies on the magnitude of $e_X(x)$, with a lower magnitude creating a larger gap between $P_X(x)$'s upper bound and 1.

From the two cases presented above, it becomes evident that the value of W determines the extent to which the projected probability $P_X(x)$ is influenced by the magnitude and proportion of evidence respectively. Specifically, a small W implies that $P_X(x)$ is predominantly influenced by the proportion of evidence distribution, whereas a large W leads $P_X(x)$ to mainly considering the magnitude of the evidence while overlooking the evidence proportion.

Intuitively speaking, for any specific case, there should exist an optimal value for W which can balance the inherent trade-off between leveraging the proportion of evidence and its magnitude to obtain predictive scores minimizing model over-confidence. However, it is unlikely that such an optimal value is universally applicable to all scenarios, given the

myriad of complex factors influencing the network's output. Hence, we advocate for relinquishing the rigidity of assigning the number of classes to W , but instead, treating W as an adjustable hyperparameter within the neural network. Therefore, as presented in Fig. 1, we revisit Eqn. 5 to derive a generalized form of the concentration parameter α_X of the constructed Dirichlet PDF:

$$\alpha_X(x) = \left(\frac{e_X(x)}{W} + \frac{1}{|\mathbb{X}|} \right) W = e_X(x) + \lambda, \quad (10)$$

where $\lambda = W/C \in \mathbb{R}_+$ is a hyperparameter. Note that the projected probability retains the same form as in Eqn. 7, i.e., $P_X(x) = \alpha_X(x)/S_X$, while the form of uncertainty mass is transformed into $u_X = \lambda C/S_X$.

4.2 Deprecating the Variance-minimizing Optimization Term in Empirical Risk

With the above generalized form of the concentration parameter, this subsection elaborates on our simplified EDL empirical risk, which directly optimizes the expectation of the constructed Dirichlet distribution, i.e., the projected probability P_X . In contrast, traditional EDL uses the MSE loss's expectation over the Dirichlet distribution as empirical risk, resulting in an additional variance-minimizing optimization term that potentially exacerbates overconfidence.

With the generalized setting of α_X in Eqn. 10, the projected probability P_X has the following variant:

$$P_X(x) = \frac{\alpha_X(x)}{S_X} = \frac{e_X(x) + \lambda}{\sum_{x' \in \mathbb{X}} e_X(x') + C\lambda}, \quad \forall x \in \mathbb{X}. \quad (11)$$

Consequently, by substituting the class probability in traditional MSE loss with the projected probability P_X in Eqn. 11, we seamlessly derive our empirical risk denoted $\mathcal{L}_{\text{re-edl-emp}}$:

$$\mathcal{L}_{\text{re-edl-emp}} = \frac{1}{|\mathcal{D}|} \sum_{(z, \mathbf{y}) \in \mathcal{D}} \sum_{x \in \mathbb{X}} (\mathbf{y}_x - P_X(x))^2. \quad (12)$$

Regarding the reason for adopting this formulation, we contend that the projected probability P_X has the unique property of alleviating the overconfidence typically arising from optimization toward the hard one-hot labels \mathbf{y} . As previously noted, the projected probability P_X harnesses both the magnitude and proportion of collected evidence to more accurately represent the actual likelihood of a given output. From an optimization perspective, compared to the proportion of evidence among classes, i.e., $e_X(x)/\sum_x e_X(x)$, or the belief mass b_X , the projected probability P_X has more tolerance towards the existence of the uncertainty mass u_X , since u_X also contributes to the projected probability P_X according to the base rate a_X . In other words, the item $a_X u_X$ alleviates the urgency of the projected probability P_X tending to the one-hot label \mathbf{y} when the model has not collected enough evidence, since the uncertainty mass u_X is inversely proportional to the total amount of evidence, thus mitigating the over-confidence issue to some extent.

Meanwhile, Eqn. 12 can be interpreted as encouraging the expectation of the Dirichlet distribution to converge to the provided label, since the bijection introduced in Theorem 1 has been established on the following identity:

$$P_X(x) = \mathbb{E}_{\mathbf{p}_X \sim \text{Dir}(\mathbf{p}, \alpha)}[P_X(x)], \quad (13)$$

which can be easily derived from Eqn. 11 and the property of Dirichlet distributions. Therefore, by substituting Eqn. 13 into Eqn. 12 and then comparing it with Eqn. 2, we can find that the essential difference between the two empirical risks is that, EDL uses **the expectation of the traditional MSE loss over the constructed Dirichlet PDF**, while our proposed Re-EDL directly applies **MSE on the expectation of the Dirichlet PDF**. Therefore, as shown in Fig. 1, the optimization term \mathcal{L}_{var} , which attempts to minimize the variance of the Dirichlet distribution, is deprecated:

$$\begin{aligned} \mathcal{L}_{\text{var}} &= \frac{1}{|\mathcal{D}|} \sum_{(\mathbf{z}, \mathbf{y}) \in \mathcal{D}} \sum_{x \in \mathbb{X}} \text{Var}_{\mathbf{p}_X \sim \text{Dir}(\mathbf{p}_X, \boldsymbol{\alpha}_X)}[\mathbf{p}_X(x)] \\ &= \frac{1}{|\mathcal{D}|} \sum_{(\mathbf{z}, \mathbf{y}) \in \mathcal{D}} \frac{S_X^2 - \sum_{x \in \mathbb{X}} \alpha_X^2(x)}{S_X^2(S_X + 1)}. \end{aligned} \quad (14)$$

Let us delve deeper into this variance-minimizing optimization term. When the variance of a Dirichlet distribution is close to zero, the Dirichlet probability density function is in the form of a Dirac delta function which is infinitely high and infinitesimally thin. Consequently, in the entire training phase, \mathcal{L}_{var} keeps requiring an infinite amount of evidence of the target class, which further intensifies the serious over-confidence issue we seek to mitigate. From another perspective, the Dirichlet distribution which models the distribution of first-order probabilities would gradually degenerate to a traditional point estimation of first-order probabilities when its variance approaches zero, thus losing the advantage of subjective logic in modeling second-order uncertainty. Therefore, we posit that omitting \mathcal{L}_{var} contributes to alleviating the over-confidence issue which commonly results in suboptimal uncertainty estimation, while preserving the merits of subjective logic. Our ablation study further corroborates this assertion.

4.3 Delving into KL-divergence-minimizing Regularization on Non-target Evidence in Structural Risk

Originating from the pioneer work [9], a Kullback-Leibler (KL) divergence-minimizing regularization is commonly incorporated into the structural risk of EDL-related methods [12], [29], [44], [46], [53]–[55], [77]–[80], suppressing the evidence for non-target classes. While this regularization can marginally improve classification accuracy with a carefully tuned coefficient and enhance generalization on noisy data, we regard it as nonessential, since it is not mandated by subjective logic and typically brings minimal benefit on uncertainty estimation. In this subsection, we initially present the vanilla form of this regularization and its variant with our relaxation proposed in Section 4.1, and then offer an analysis of both the optimization direction and practical impact, supported by experimental results.

In the traditional EDL method, after the target class value of the Dirichlet parameter vector being set to 1, the KL divergence between the modified Dirichlet distribution and a uniform distribution is expected to be minimized by an auxiliary regularization, which has the following form:

$$\mathcal{L}_{\text{kl}} = \frac{1}{|\mathcal{D}|} \sum_{(\mathbf{z}, \mathbf{y}) \in \mathcal{D}} \text{KL}(\text{Dir}(\mathbf{p}_X, \tilde{\boldsymbol{\alpha}}_X), \text{Dir}(\mathbf{p}_X, \mathbf{1})), \quad (15)$$

where $\mathbf{1}$ denotes a C -dimensional ones vector, and $\tilde{\boldsymbol{\alpha}}_X = \mathbf{y} + (\mathbf{1} - \mathbf{y}) \odot \boldsymbol{\alpha}_X$ represents the modified Dirichlet parameter vector. Besides, an annealing coefficient $\mu_t =$

TABLE 1: The influence of \mathcal{L}_{kl} on evidence allocation and model performances on CIFAR-10. The annealing coefficient $\mu_t = \min(1.0, t/10)$ is adopted.

Methods	\mathcal{L}_{kl}	Evidence Per Testing Sample				Performance	
		Target Evidence	Non-target Evidence	Target / Total	OOD Evidence	Cls Acc	OOD Detect
EDL	✓	282.85	1.74	99.39%	28.95	88.48	82.32
	✗	1122.65	49.13	95.81%	470.99	90.20	84.50
Re-EDL	✓	69.80	0.61	99.13%	9.52	90.09	83.73
	✗	829.51	31.56	96.33%	302.34	90.13	85.46

$\min(1.0, t/10) \in [0, 1]$ is adopted for this regularization, where t is the training epoch index. In the case of adopting the relaxation of the prior weight W in Eqn. 10, the Dirichlet distribution bijective to the vacuous opinion $\tilde{\boldsymbol{\omega}}_X = (\mathbf{b}_X = \mathbf{0}, u_X = 1)$ is no longer a uniform distribution. Specifically, it is parameterized by $\lambda \cdot \mathbf{1}$, and \mathcal{L}_{kl} is modified into:

$$\begin{aligned} \mathcal{L}_{\text{kl}}(\lambda) &= \frac{1}{|\mathcal{D}|} \sum_{(\mathbf{z}, \mathbf{y}) \in \mathcal{D}} \text{KL}(\text{Dir}(\mathbf{p}_X, \tilde{\boldsymbol{\alpha}}_X^\lambda), \text{Dir}(\mathbf{p}_X, \lambda \cdot \mathbf{1})) \\ &\approx \frac{1}{|\mathcal{D}|} \sum_{(\mathbf{z}, \mathbf{y}) \in \mathcal{D}} \left(\log \frac{\Gamma(\tilde{S}_X^\lambda)}{\prod_{x \in \mathbb{X}} \Gamma(\tilde{\alpha}_X^\lambda(x))} + \right. \\ &\quad \left. \sum_{x \in \mathbb{X}} (\tilde{\alpha}_X^\lambda(x) - \lambda) (\psi(\tilde{\alpha}_X^\lambda(x)) - \psi(\tilde{S}_X^\lambda)) \right), \end{aligned} \quad (16)$$

where Γ and ψ denote the gamma and digamma functions, $\tilde{\boldsymbol{\alpha}}_X^\lambda = \lambda \mathbf{y} + (\mathbf{1} - \mathbf{y}) \odot \boldsymbol{\alpha}_X$, and $\tilde{S}_X^\lambda = \sum_{x \in \mathbb{X}} \tilde{\alpha}_X^\lambda(x)$. The detailed derivation is in Appendix A.2. With the introduction complete, we proceed to conduct an in-depth analysis of the KL-Div-minimizing regularization from following aspects.

Theoretically, does the optimization direction of this regularization align with the common sense? It is unlikely to be the case. As introduced by [9], this regularization is motivated by the principle that “we prefer the total evidence to shrink to zero for a sample if it cannot be correctly classified”. However, the actual impact of \mathcal{L}_{kl} extends far beyond the motivation: Since both Eqn. 15 and Eqn. 16 achieve their unique minimum value when $\tilde{\boldsymbol{\alpha}}_X = \mathbf{1}$ or $\tilde{\boldsymbol{\alpha}}_X^\lambda = \lambda \cdot \mathbf{1}$, this regularization not only affects misclassified samples but also encourages the evidence for all non-target classes to approach zero for all training samples. As clearly shown in Table 1, the magnitudes of non-target evidence diminishes substantially when \mathcal{L}_{kl} is adopted. We argue that this optimization direction contradicts common sense, particularly on challenging samples. For instance, it is reasonable for a network model or a human analyst to gather some evidence supporting the classification of a poorly written digit “3” as an “8” or categorizing a dog-like “cat” as a “dog” due to their shared visual patterns. In other words, since there is an inevitable overlap in visual patterns among different categories (otherwise, classification would be extremely easy), the situation where all non-target evidence, as a proxy of non-target belief mass, shrinks to zero should not occur.

Empirically, how does this regularization influence evidence distributions and uncertainty estimation? As presented in Table 1, when \mathcal{L}_{kl} is adopted, the total evidence for non-target categories is suppressed to nearly zero. Since the direct optimization target of the loss function is the probability distribution, the magnitude of the target class evidence also decreases due to the influence of minimal non-target class evidence. However, the ratio of the target class

evidence to total evidence increases, which is positively correlated with the projected probability P_X , rising from about 96% without the use of \mathcal{L}_{kl} to over 99% with it. Therefore, the increase in this ratio indicates a substantial escalation in the model’s overconfidence, which is specifically reflected in the decrease in OOD detection performance shown in Table 1 and Table 8. From an informational perspective, when the evidence for non-target classes vanishes, the potentially useful information carried by the magnitude of evidence is also lost, thereby impairing the model’s capability.

Does this regularization always lead to worse results?

No, not always. While in most cases we observe a decrease in OOD detection performance when adopting \mathcal{L}_{kl} , this regularization may bring slight improvements on classification accuracy with a carefully tuned coefficient. Additionally, our experiments demonstrates that this regularization provides strong generalization ability when encountering noisy testing data. We deduce that this benefit arises from \mathcal{L}_{kl} functioning similarly to standard L1/L2 regularization. While L1/L2 regularization directly limits the magnitude of model parameters to reduce model complexity, \mathcal{L}_{kl} indirectly constrains model parameters by suppressing the magnitude of model’s outputs (both target and non-target evidence) within a narrower range, thus also reducing complexity and mitigating overfitting. Furthermore, existing studies [51], [53], [81] have explored variants of regularization on non-target evidence, which possess unique properties and have been proven effective in various applications. Despite that we refer to it as a nonessential setting and, as shown in Fig. 1, derive the Re-EDL method by removing it, we believe this type of regularization is effective in certain cases and warrants further exploration.

4.4 What are the Essential Settings of EDL?

In Section 4.1, we challenge the rigidity of fixing the prior weight to the class number, advocating instead for treating it as an adjustable hyperparameter. In Section 4.2, we propose a simplified empirical risk by deprecating a variance-minimizing optimization term in the traditional EDL loss. In Section 4.3, we analyze the disadvantages of the commonly used KL-Div-minimizing regularization on non-target evidence. With these relaxations, our EDL variant, Re-EDL, simply optimizes the expectation of the constructed Dirichlet distribution, also known as the projected probability, using the given one-hot labels, without any additional regularization. The impressive simplicity of the Re-EDL formulation naturally leads to a fundamental question: **What is the essential EDL setting that contributes to its uncertainty estimation capability?**

Our experiments shows that, simply replacing the traditional softmax probability with the projected probability in traditional CE and MSE loss functions results in obvious improvements ($> 4\%$) in OOD detection performances (refer to Table 11). Therefore, in this subsection, we argue that **the adoption of the projected probability** is the essential setting of EDL, and delve into its differences with the traditional softmax probability. For the convenience of following discussion, we first present their formulations here:

$$\text{Softmax Probability}_x = \frac{\exp(l_x)}{\sum_{x' \in \mathbb{X}} \exp(l_{x'})}, \quad (17)$$

$$\begin{aligned} \text{Projected Probability}_x &= \frac{\text{softplus}(l_x)}{\underbrace{\sum_{x' \in \mathbb{X}} \text{softplus}(l_{x'}) + |\mathbb{X}| \cdot \lambda}_{\text{Belief mass } \mathbf{b}_X(x)}} \\ &+ \underbrace{\frac{1}{|\mathbb{X}|}}_{\text{Base rate } \mathbf{a}_X(x)} \cdot \underbrace{\frac{|\mathbb{X}| \cdot \lambda}{\sum_{x' \in \mathbb{X}} \text{softplus}(l_{x'}) + |\mathbb{X}| \cdot \lambda}}_{\text{Uncertainty mass } u_X} \quad (18) \\ &= \frac{\text{softplus}(l_x) + \lambda}{\sum_{x' \in \mathbb{X}} (\text{softplus}(l_{x'}) + \lambda)}, \end{aligned}$$

where l_x represents the x -th value of the output logit vector.

After simplification, the differences between Eqn. 17 and Eqn. 18 lies in: **(1)** Class scores in the projected probability include an additional parameter λ ; **(2)** The projected probability replaces the exponential function with softplus for activation. As shown in Table 10, both modifications result in an obvious improvement in OOD detection performance compared to the softmax classification head, without incurring any additional computational cost. We argue that the underlying reasons for the improvement brought by the two modifications are unified: **it better utilizes the magnitude information carried by the model’s output logits.**

First, the extra parameter λ ensures that the information carried by the magnitude of logits is partially preserved during the normalization of the predicted probability distributions. As discussed in Section 4.1, in the EDL framework, the value of prior weight determines the extent to which the projected probability is influenced by the magnitude and proportion of evidence, respectively. When the prior weight W vanishes to zero ($\lambda = W/|\mathbb{X}| = 0$), the projected probability is solely determined by the proportion of the evidence distribution, disregarding their magnitudes. However, this is exactly what consistently occurs in the softmax probability lacking the extra parameter: class scores $[e^5, e^3, e^2]$ are indistinguishable from $[e^0, e^{-2}, e^{-3}]$ after normalization, despite the significant difference in their magnitudes. By introducing an appropriate parameter λ to the class scores, as demonstrated in Table 10, the model obtains the opportunity to leverage the magnitude information carried by logits, which potentially benefits uncertainty estimation.

Secondly, projected probability replaces the exponential function with an activation function that has a more gradual growth rate, mitigating the severe overconfidence issue in softmax probability, which heavily favors one class over others. Due to the nature of exponentiation, the softmax operation tends to amplify larger logits and suppress smaller ones, transforming logit distributions with diverse magnitude information to homogeneous, nearly one-hot probability distributions. In contrast, softplus offers a gentler growth rate and better preserving magnitude information of logits.

Theoretically, softplus is not the only choice for the evidence function. Subjective logic only requires the belief mass to be within the range of 0 to 1, meaning the evidence needs to be non-negative. Hence, in the EDL framework, this function only needs to ensure non-negativity, and options like ReLU, softplus, and even Exp all meet this criterion. However, Exp’s exponential growth rate transforms probability distributions into forms close to one-hot, while ReLU is rarely used for activation in the output layer of modern neural networks because it crudely zeros out all negative logits and causes serious information loss. For implementation, we deduce that non-negative functions similar to

TABLE 2: Performance comparison evaluated by classification accuracy and AUPR scores for OOD detection on CIFAR-10. $\rightarrow X$ indicates using X as OOD data. Results are averaged over 5 runs, with mean and standard deviation reported, except for the deep ensemble method which uses 25 model instances.

Method	CIFAR10		\rightarrow SVHN	\rightarrow CIFAR100	\rightarrow GTSRB	\rightarrow LFWPeople	\rightarrow Places365	\rightarrow Food101	Mean
	Cls Acc	Mis Detect	OOD Detect	OOD Detect	OOD Detect	OOD Detect	OOD Detect	OOD Detect	OOD Detect
MC Dropout [5]	90.16±0.23	98.86±0.06	78.40±3.88	85.39±0.58	83.51±2.32	87.98±2.74	67.63±2.34	76.07±2.58	79.83±2.41
EDL [9]	88.48±0.32	98.74±0.07	82.32±1.21	87.13±0.26	84.57±1.26	89.26±1.70	70.46±0.77	80.18±0.69	82.32±0.98
DUQ [71]	89.39±0.13	97.98±0.34	81.44±4.63	85.38±0.37	83.35±4.30	88.96±4.06	66.20±3.61	75.87±4.40	80.20±3.56
PostN [75]	87.82±0.06	97.46±0.06	83.76±0.46	87.07±0.94	84.83±1.67	88.76±3.08	71.79±2.36	78.83±2.53	82.51±1.84
NatPN [76]	87.73±0.09	97.53±0.05	83.56±0.38	86.98±0.75	84.76±2.03	88.85±2.86	71.14±2.10	79.04±2.66	82.39±1.80
RED [28]	89.43±0.28	98.82±0.09	82.85±2.35	87.84±0.54	85.30±3.81	89.15±2.90	70.78±2.33	79.91±1.92	82.64±2.31
\mathcal{I} -EDL [29]	88.38±0.15	98.71±0.11	84.97±2.11	86.31±0.32	84.79±2.13	89.34±0.98	68.92±1.21	77.75±2.07	82.01±1.47
R-EDL [21]	90.09±0.31	98.98±0.05	85.00±1.22	87.73±0.31	87.25±0.69	90.79±1.15	71.97±0.69	79.64±2.36	83.73±1.07
Re-EDL	90.13±0.25	98.81±0.05	89.94±1.40	88.31±0.16	90.53±2.04	89.71±2.08	73.42±1.05	80.83±1.72	85.46±1.41
Deep Ensemble(5) [6]	92.55±0.14	99.32±0.03	84.77±1.42	89.15±0.15	88.01±1.22	90.40±0.80	73.89±0.62	80.60±1.00	84.47±0.87
Re-EDL+Deep Ensemble(5)	92.76±0.11	99.34±0.02	92.64±0.35	90.55±0.13	92.52±0.91	92.08±0.96	77.31±0.27	84.96±0.42	88.35±0.51
Deep Ensemble(25)	93.01	99.44	86.22	90.17	89.77	90.77	75.92	82.45	85.88
Re-EDL+Deep Ensemble(25)	93.27	99.46	93.45	91.01	93.07	92.29	78.13	85.82	88.96

softplus, i.e., those that maintain a gradual but non-zero growth rate over the entire real number domain, are likely to be more effective in preserving magnitude information.

In summary, the essential setting of EDL is replacing softmax with the projected probability, which adds a proper extra parameter to class scores and uses an output activation function with a more gradual growth rate instead of Exp, thereby better preserving useful magnitude information of logits and improving uncertainty estimation.

5 EXPERIMENTS

5.1 Experimental Setup

Baselines. Following [29], we focus on comparing with other Dirichlet-based uncertainty methods, including the traditional EDL [9], \mathcal{I} -EDL [29], RED [28], R-EDL [21], PostN [75], and NatPN [76]. Additionally, we present the results of the representative single-forward-pass method DUQ [71], the popular Bayesian uncertainty method MC Dropout [5], and the Deep Ensemble [6] method using 5 and 25 model instances for reference. For experiments concerning video-modality data, following [11], we compare our methods with: OpenMax [82], MC Dropout, BNN SVI [83], RPL [84], and DEAR [11].

Datasets. Refer to Appendix B.2 for a detailed introduction.

5.2 Implementation Details

Classical setting. Six datasets (i.e., SVHN [85], CIFAR-100 [86], GTSRB [87], LFWPeople [88], Places365 [89], Food-101 [90]) are utilized as OOD data for CIFAR-10, while FMNIST [91] and KMNIST [92] are used for MNIST. In alignment with [29], [75], VGG16 serves as the backbone network for CIFAR-10, and a ConvNet with three convolutional and three dense layers is employed for MNIST. Softplus is adopted as the evidence function. The Adam optimizer is employed with a learning rate of 1×10^{-4} for CIFAR-10, and a learning rate of 1×10^{-3} , decaying by 0.1 every 15 epochs for MNIST. The hyperparameter λ is set to 0.8 and 0.1 for CIFAR-10 and MNIST, which is selected from the range [0.1:0.1:1.0] on the validation set. The batch size is set to 64, and the training epoch is set to 200 and 60 for CIFAR-10 and MNIST. Reported results are averaged over 5 runs.

Few-shot setting. Following [29], we adopt a pre-trained WideResNet-28-10 network from [93] to extract features and

train a single dense layer for experiments under a challenging few-shot setting on the mini-ImageNet [94] dataset, with the testing set of CUB [95] as OOD data. We employ the N -way K -shot setting, with $N \in \{5, 10\}$ and $K \in \{1, 5, 20\}$. Each few-shot episode comprises N random classes and K random samples per class for training, $\min(15, K)$ query samples per class from mini-ImageNet for classification and confidence estimation, and an equivalent number of query samples from the CUB dataset for OOD detection. Reported results are averaged over 10,000 episodes. Softplus is used as the activation function to keep evidence non-negative. The LFBFGS optimizer is employed with the default learning rate 1.0 for 100 epochs. The hyperparameter λ is also selected on the meta-validation set, as shown in Table 14 in Appendix.

Video-modality setting. Following [11], we investigate the open-set action recognition task on UCF-101 [96] using I3D as the backbone network. HMDB-51 [97] and MiT-v2 [98] serve as sources of unknown samples. The hyperparameter λ is set to 0.8, with a batch size of 8.

Noisy setting. To evaluate the model’s generalization on noisy data, we generate noisy samples by adding zero-mean Gaussian noises with standard deviations of [0.025:0.025:0.200] to the testing samples of CIFAR-10.

Other details. All experiments were conducted on NVIDIA RTX 3090 GPUs using Python 3.8 and PyTorch 1.12. The source code link is provided in the abstract.

5.3 Classical Setting

A classifier with reliable uncertainty estimation abilities should assign higher uncertainties to out-of-distribution (OOD) than in-distribution (ID) samples, assign higher uncertainties to misclassified than to correctly classified samples, as well as maintain comparable classification accuracy. Therefore, we evaluate our method by OOD detection and misclassification detection in image classification, measured by the area under the precision-recall curve (AUPR) with labels 1 for ID data, and labels 0 for OOD data. For the Dirichlet-base uncertainty methods, we use (the reciprocal of) uncertainty mass as the confidence scores, while for methods which do not involve Dirichlet PDFs, we use the max probability. As shown in Table 2, R-EDL and Re-EDL consistently exhibit superior performance across most metrics. Specifically, when compared with the traditional

TABLE 3: AUPR scores of OOD detection in the classical setting, measured by MP (Max projected probability), UM (Uncertainty Mass), DE (Differential Entropy), and MI (Mutual Information). Please note that this table provides detailed results for specific methods; for a comprehensive overview of all baselines, refer to Table 2.

Method	CIFAR10→SVHN				CIFAR10→CIFAR100				CIFAR10→GTSRB			
	MP	UM	DE	MI	MP	UM	DE	MI	MP	UM	DE	MI
EDL	82.30±1.17	82.32±1.21	82.30±1.18	82.32±1.21	87.15±0.25	87.13±0.25	87.15±0.26	87.13±0.26	84.59±1.27	84.57±1.26	84.60±1.27	84.58±1.26
\mathcal{I} -EDL	85.11±2.29	84.97±2.11	85.12±2.29	84.98±2.12	86.36±0.31	86.31±0.32	86.37±0.31	86.31±0.32	84.90±2.15	84.79±2.14	84.91±2.15	84.80±2.14
R-EDL	85.00±1.22	85.00±1.22	85.01±1.14	85.00±1.22	87.72±0.31	87.73±0.31	87.61±0.33	87.73±0.31	87.25±0.68	87.25±0.69	87.16±0.63	87.25±0.68
Re-EDL	87.84±0.96	89.94±1.40	89.34±1.31	89.89±1.39	87.57±0.23	88.31±0.16	88.16±0.17	88.30±0.16	89.14±1.69	90.53±2.04	90.17±1.96	90.50±2.03

Method	CIFAR10→LFWPeople				CIFAR10→Places365				CIFAR10→Food101			
	MP	UM	DE	MI	MP	UM	DE	MI	MP	UM	DE	MI
EDL	89.26±1.67	89.26±1.70	89.25±1.68	89.26±1.70	70.47±0.78	70.46±0.77	70.48±0.78	70.46±0.77	80.19±0.69	80.18±0.69	80.19±0.69	80.18±0.69
\mathcal{I} -EDL	89.33±0.99	89.34±0.98	89.32±0.99	89.34±0.99	68.95±1.19	68.92±1.21	68.97±1.20	68.92±1.21	77.88±2.10	77.75±2.07	77.89±2.09	77.76±2.07
R-EDL	90.79±1.15	90.79±1.15	90.82±1.14	90.79±1.15	71.97±0.69	71.97±0.69	71.84±0.70	71.97±0.69	79.64±2.36	79.64±2.36	79.57±2.38	79.64±2.36
Re-EDL	89.75±2.08	89.71±2.08	89.72±2.09	89.71±2.08	72.27±1.03	73.42±1.05	73.09±1.04	73.39±1.05	79.97±1.61	80.83±1.72	80.56±1.67	80.81±1.71

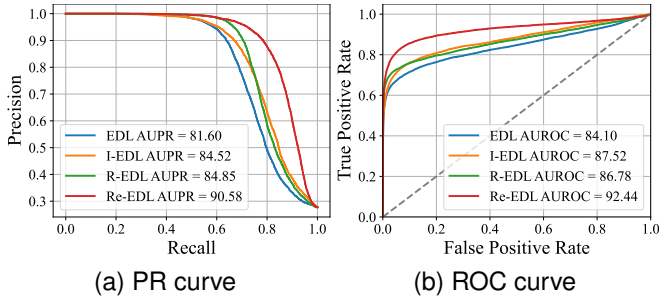


Fig. 2: Precision-Recall (PR) curves and Receiver Operating Characteristic (ROC) curves of differentiating OOD data (SVHN) from ID data (CIFAR-10) in the classical setting. The adopted uncertainty measure is uncertainty mass (UM).

EDL method [9] and the newly proposed \mathcal{I} -EDL [29], R-EDL achieves absolute gains of 1.41% and 1.72% AUPR averaged over six OOD datasets, by relaxing the nonessential settings on prior weight and deprecating the variance-minimizing optimization term. Re-EDL offers even greater improvements, with gains of 3.14% and 3.45%, by further deprecating the KL-Div-minimizing regularization on non-target evidence. Moreover, as a single-forward-pass method, Re-EDL can be easily integrated into deep ensemble [6] to enhance performance, albeit at a multiplicative computational cost. According to Table 2, when incorporated into the deep ensemble method using 5 and 25 model instances, our proposed Re-EDL achieves enhancements of 3.88% and 3.08%, respectively, in the averaged AUPR of OOD detection, alongside modest improvements in classification accuracy and misclassification detection. All results are averaged over five runs to mitigate effects of randomness.

Moreover, we present AUPR scores of OOD detection using various uncertainty measures, including MP (Max projected Probability), UM (Uncertainty Mass), DE (Differential Entropy), and MI (Mutual Information), in Table 3, and AUROC scores in Table 15 (Appendix C.1). Derivations of these measures can be found in Appendix A.3. In Fig. 2, we present the Precision-Recall (PR) curves and Receiver Operating Characteristic (ROC) curves of differentiating OOD data (SVHN) from ID data (CIFAR-10) using UM as the uncertainty measure. Curves with other measures are plotted in Fig. 4 and Fig. 5 (Appendix C.1). Table 4 shows results on MNIST, with FMNIST and KMNIST as OOD data. These results further validate the effectiveness of Re-EDL.

TABLE 4: Results on MNIST, averaged over 5 runs. ConvNet consisting of 3 conventional layers and 3 dense layers is adopted as the backbone network.

Method	MNIST		→KMNIST	→FMNIST
	Cls Acc	Mis Detect	OOD Detect	OOD Detect
MC Dropout	99.30±0.05	99.98±0.02	98.09±0.12	98.73±0.41
DUQ	98.65±0.12	99.97±0.03	98.52±0.11	97.92±0.60
PostN	99.29±0.04	99.97±0.03	94.62±0.24	97.28±0.37
EDL	98.22±0.31	99.98±0.00	96.31±2.03	98.08±0.42
\mathcal{I} -EDL	99.21±0.08	99.98±0.00	98.33±0.24	98.86±0.29
R-EDL	99.33±0.03	99.99±0.00	98.69±0.20	99.29±0.12
Re-EDL	99.35±0.00	99.99±0.00	99.03±0.28	99.65±0.09

5.4 Few-shot Setting

Next, we conduct more challenging few-shot experiments on mini-ImageNet to further demonstrate the effectiveness of our method. As shown in Table 5, we report the averaged top-1 accuracy of classification and the AUPR scores of confidence estimation and OOD detection over 10,000 few-shot episodes. As depicted in Table 5, R-EDL and Re-EDL achieve satisfactory performances on most N -way K -shot settings. Specifically, comparing with the EDL and \mathcal{I} -EDL methods, R-EDL obtains absolute gains of 9.19% and 1.61% when evaluated by MP on OOD detection of the 5-way 5-shot task. However, in this setting, Re-EDL fail to achieve further improvements over R-EDL as it does in the classical setting and subsequent video-modality setting. We speculate that this may be because few-shot tasks demand stronger generalization capabilities due to the limited amount of training data. Consequently, the improvement in generalization brought about by the KL-Divergence-minimizing regularization compensates for the performance loss it otherwise causes. However, after deprecating this regularization, our simpler Re-EDL still achieves performances comparable to those of R-EDL in the few-shot setting, which also suggests that the regularization is not an essential EDL setting.

5.5 Video-modality Setting

We also assess our approach using video-modality samples [11], [99], specifically on the open-set action recognition task. Following [11], we train models on UCF-101 training split and use the testing splits of HMDB-51 and MiT-v2 datasets as unknown sources. Given that the SOTA method DEAR is predicated on EDL, we substitute its EDL implementation with our R-EDL and Re-EDL version. As evidenced by Table 7, this modification yields enhanced performance, substantiating the efficacy of our methods.

TABLE 5: Results of the few-shot setting for WideResNet-28-10 on mini-ImageNet, with the CUB dataset as OOD data.

Method	5-Way 1-Shot				5-Way 5-Shot				5-Way 20-Shot			
	Cls Acc	Mis Detect	OOD-MP	OOD-UM	Cls Acc	Mis Detect	OOD-MP	OOD-UM	Cls Acc	Mis Detect	OOD-MP	OOD-UM
EDL	61.00±0.11	75.34±0.12	66.78±0.12	65.41±0.13	80.38±0.08	92.09±0.05	74.46±0.10	76.53±0.14	85.54±0.06	97.05±0.02	80.01±0.10	79.78±0.12
\mathcal{I} -EDL	63.82±0.10	80.33±0.11	71.79±0.12	74.76±0.13	82.00±0.07	93.61±0.05	82.04±0.10	82.48±0.10	88.12±0.05	96.98±0.02	84.29±0.09	85.40±0.09
R-EDL	63.93±0.11	80.80±0.11	72.91±0.12	74.84±0.13	81.85±0.07	93.65±0.05	83.65±0.10	84.22±0.10	88.74±0.05	97.10±0.02	84.85±0.09	85.57±0.09
Re-EDL	63.64±0.10	80.65±0.11	73.20±0.12	75.61±0.13	82.05±0.07	93.75±0.05	83.10±0.10	83.35±0.10	88.32±0.05	96.39±0.03	85.15±0.09	86.06±0.09

Method	10-Way 1-Shot				10-Way 5-Shot				10-Way 20-Shot			
	Cls Acc	Mis Detect	OOD-MP	OOD-UM	Cls Acc	Mis Detect	OOD-MP	OOD-UM	Cls Acc	Mis Detect	OOD-MP	OOD-UM
EDL	44.55±0.08	61.68±0.10	59.19±0.09	67.81±0.12	62.50±0.08	84.35±0.06	71.06±0.10	76.28±0.10	69.30±0.09	93.15±0.03	74.50±0.08	76.89±0.09
\mathcal{I} -EDL	49.37±0.07	67.54±0.09	71.60±0.10	71.95±0.10	67.89±0.06	85.52±0.05	80.63±0.11	82.29±0.10	78.59±0.04	93.32±0.03	81.34±0.07	82.52±0.07
R-EDL	50.02±0.07	67.12±0.09	72.83±0.10	73.08±0.10	70.51±0.05	86.26±0.05	82.39±0.09	83.37±0.09	79.79±0.04	93.47±0.02	82.22±0.08	82.72±0.07
Re-EDL	50.69±0.07	68.47±0.09	71.48±0.10	71.39±0.10	69.38±0.05	85.79±0.05	82.46±0.09	83.33±0.08	78.79±0.04	91.20±0.04	82.79±0.07	84.09±0.07

TABLE 6: Results of the noisy setting on CIFAR-10, averaged over 5 seeds. Noisy samples are generated by adding zero-mean Gaussian noises with standard deviations of [0.025:0.025:0.200] to the testing samples of CIFAR-10.

SD of Noise	0.025			0.050			0.075			0.100		
Method	Cls Acc	Noisy Detect	Avg	Cls Acc	Noisy Detect	Avg	Cls Acc	Noisy Detect	Avg	Cls Acc	Noisy Detect	Avg
EDL	86.26±0.44	52.78±0.23	69.52	75.38±1.11	62.75±0.65	69.07	58.13±3.04	72.98±1.44	65.56	41.87±3.98	79.10±2.24	60.48
\mathcal{I} -EDL	85.80±0.56	52.91±0.47	69.36	73.40±2.25	62.12±1.38	67.76	56.78±3.77	70.32±1.35	63.55	43.62±4.42	75.58±0.58	59.60
R-EDL	87.54±0.35	53.48±0.55	70.51	76.35±1.56	64.19±1.02	70.27	60.19±3.03	75.33±1.43	67.76	45.70±3.67	82.97±1.54	64.34
Re-EDL	87.37±0.64	53.18±0.18	70.28	75.76±1.72	62.69±0.71	69.22	59.68±3.04	72.94±1.34	66.31	44.22±2.60	80.24±1.89	62.23

SD of Noise	0.125			0.150			0.175			0.200		
Method	Cls Acc	Noisy Detect	Avg	Cls Acc	Noisy Detect	Avg	Cls Acc	Noisy Detect	Avg	Cls Acc	Noisy Detect	Avg
EDL	30.45±4.27	82.07±2.85	56.26	23.45±4.00	83.77±3.20	53.61	19.51±3.77	85.13±3.34	52.32	17.15±3.35	86.45±3.31	51.80
\mathcal{I} -EDL	34.58±4.52	79.31±1.15	56.94	28.56±4.35	82.13±2.23	55.34	24.45±4.14	84.29±3.12	54.37	21.57±3.69	85.97±3.69	53.77
R-EDL	35.16±2.97	87.62±1.49	61.39	28.47±1.87	90.50±1.55	59.48	24.07±2.08	92.32±1.86	58.20	20.83±2.50	93.50±2.24	57.16
Re-EDL	33.85±1.69	84.61±2.29	59.23	27.00±1.61	87.16±2.65	57.08	22.83±2.59	88.72±3.10	55.78	19.90±3.34	89.76±3.68	54.83

TABLE 7: Results of video-modality setting for I3D backbone on UCF-101, with HMDB-51 and MiT-v2 as OOD data. Results of baselines are reported by [11].

Method	UCF-101→HMDB-51		UCF-101→MiT-v2	
	Open maF1	Open Set AUC	Open maF1	Open Set AUC
OpenMax	67.85±0.12	74.34	66.22±0.16	77.76
MC Dropout	71.13±0.15	75.07	68.11±0.20	79.14
BNN SVI	71.57±0.17	74.66	68.65±0.21	79.50
SoftMax	73.19±0.17	75.68	68.84±0.23	79.94
RPL	71.48±0.15	75.20	68.11±0.20	79.16
DEAR	77.24±0.18	77.08	69.98±0.23	81.54
R-EDL	78.73±0.15	77.94	70.85±0.25	82.26
Re-EDL	78.92±0.13	78.02	71.03±0.21	82.39

5.6 Noisy Setting

In Section 4.3, we argue that the regularization \mathcal{L}_{kl} constrains the magnitude of model outputs within a narrower range, thereby reducing complexity and mitigating overfitting to some extent. Although \mathcal{L}_{kl} typically has a negative effect in experiments across the classical and video-modality settings, it exhibits strong generalization capabilities when tested on noisy data. Specifically, we introduce zero-mean isotropic Gaussian noise into the test split of the ID dataset to generate noisy samples. Table 6 presents the classification accuracy and the AUPR scores for noisy detection across varying levels of Gaussian noise on CIFAR-10. As indicated in Table 6, R-EDL significantly outperforms both EDL and \mathcal{I} -EDL across nearly all noise levels, with its advantages becoming more pronounced as the noise intensity increases. However, the performance of Re-EDL, which omits the KL-Div-minimizing regularization, generally falls below that of R-EDL. This observation suggests that \mathcal{L}_{kl} equips R-EDL with superior generalization abilities, enabling it to collect reliable evidence from noisy data, thereby leading to enhanced performances. Nonetheless, Re-EDL still maintains superior performances compared to both EDL and \mathcal{I} -EDL.

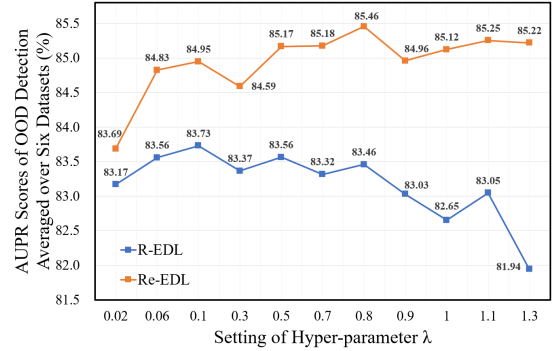


Fig. 3: Parameter analysis of the hyperparameter λ , evaluated by averaged AUPR for OOD detection on CIFAR-10.

TABLE 8: Performances on CIFAR-10 with varying values of the KL-Div-minimizing regularization coefficient μ . Note that μ here is a scalar coefficient instead of an annealing one.

$\lg \mu$	EDL		$\lg \mu$	Re-EDL	
	Cls Acc	OOD Detect		Cls Acc	OOD Detect
$-\infty$	90.20	84.50	$-\infty$	90.13	85.46
-3.0	90.12 (-0.08)	84.79 (+0.29)	-3.0	90.06 (-0.07)	84.41 (-1.05)
-2.3	90.21 (+0.01)	83.97 (-0.53)	-2.3	90.19 (+0.06)	83.81 (-1.65)
-2.0	90.22 (+0.02)	82.80 (-1.70)	-2.0	89.86 (-0.27)	83.06 (-2.40)
-1.3	90.15 (-0.06)	82.80 (-1.70)	-1.3	90.40 (+0.27)	83.20 (-2.26)
-1.0	90.22 (+0.02)	82.88 (-1.62)	-1.0	90.34 (+0.21)	83.16 (-2.30)
-0.3	89.47 (-0.73)	82.86 (-1.64)	-0.3	24.29 (-65.84)	51.43 (-34.03)
0.0	74.99 (-15.21)	76.13 (-8.37)	0.0	13.13 (-77.00)	43.86 (-41.60)
0.7	32.52 (-57.68)	46.54 (-37.96)	0.7	12.05 (-78.08)	40.33 (-45.13)

5.7 Parameter Analysis

Hyperparameter λ in projected probability. We further investigate the effect of the hyperparameter λ . Fig. 3 presents the trend of variation in the average AUPR score for OOD detection on six OOD datasets as the hyperparameter λ varies from 0.02 to 1.3. The observations reveal findings

TABLE 9: Ablation study on the classical setting, with respect to the relaxations about treating λ as a hyperparameter and deprecating the optimization term \mathcal{L}_{var} and the regularization term \mathcal{L}_{kl} .

Nonessential Settings			CIFAR10		→SVHN	→CIFAR100	→GTSRB	→LFWPeople	→Places365	→Food101	Mean
$\lambda = 1$	\mathcal{L}_{var}	\mathcal{L}_{kl}	Cls Acc	Mis Detect	OOD Detect	OOD Detect	OOD Detect	OOD Detect	OOD Detect	OOD Detect	OOD Detect
✓	✓	✓	88.48±0.32	98.74±0.07	82.32±1.21	87.13±0.26	84.57±1.26	89.26±1.70	70.46±0.77	80.18±0.69	82.32±0.98
-	✓	✓	89.33±0.18	98.94±0.03	84.77±1.82	87.62±0.15	87.68±1.09	90.31±1.86	71.68±1.27	80.41±0.90	83.75±1.18
✓	-	✓	88.25±0.29	98.73±0.04	84.30±1.56	86.90±0.33	84.44±0.33	88.40±2.18	69.79±1.56	80.33±0.98	82.36±1.43
✓	✓	-	<u>90.20±0.09</u>	98.78±0.02	88.05±1.95	88.17±0.22	88.87±1.36	88.41±2.84	75.20±0.77	78.33±1.96	84.50±1.52
-	-	✓	90.09±0.31	98.98±0.05	85.00±1.22	87.73±0.31	87.25±0.69	90.79±1.15	71.97±0.69	79.64±2.36	83.73±1.07
-	✓	-	90.25±0.23	98.78±0.07	87.30±1.38	88.45±0.39	87.99±3.05	89.07±1.84	74.86±0.85	79.22±3.13	84.48±1.77
✓	-	-	90.19±0.14	98.82±0.06	<u>88.93±1.11</u>	88.29±0.11	<u>89.46±1.20</u>	90.24±0.85	73.45±0.72	80.33±0.92	<u>85.12±0.82</u>
-	-	-	90.13±0.25	98.81±0.05	89.94±1.40	<u>88.31±0.16</u>	90.53±2.04	89.71±2.08	73.42±1.05	80.83±1.72	85.46±1.41

TABLE 10: Ablation study of the essential EDL setting. Experimental settings keep consistent with Table 1.

Methods	Class Score		Activation Function		Performance	
	Vanilla	Extra λ	Exponential	Softplus	Cls Acc	OOD Detect
Softmax	✓	-	✓	-	90.10±0.25	81.30±2.36
Re-EDL ($\lambda = 0$)	✓	-	-	✓	90.08±0.10	83.48±2.11
Re-EDL (Exp)	-	✓	✓	-	89.81±0.18	82.39±2.03
Re-EDL	-	✓	-	✓	90.13±0.25	85.46±1.41

TABLE 11: Validation of the essential EDL setting in the cross-entropy (CE) loss formulation by simply replacing softmax classification head with projected probability.

Loss	Method	CIFAR10 Cls Acc	→SVHN OOD Detect	→CIFAR100 OOD Detect	Mean (six datasets) OOD Detect
CE	Softmax	90.11±0.19	80.05±3.04	85.86±0.67	80.33±2.70
	Re-EDL	90.48±0.25	<u>85.54±1.29</u>	88.65±0.37	<u>84.56±1.00</u>
MSE	Softmax	90.10±0.25	83.62±3.29	86.54±0.18	81.30±2.36
	Re-EDL	90.13±0.25	89.94±1.40	<u>88.31±0.16</u>	85.46±1.41

in two aspects. On one hand, examining the two curves individually, the hyperparameter λ has a noticeable impact on OOD detection performance, with the effect varying by nearly 2% within the range of 0.02 to 1.3. Fixing the prior weight to the number of classes, i.e., setting λ to 1, typically fails to achieve optimal performance. On the other hand, when comparing the performance gap between the two curves, removing \mathcal{L}_{kl} consistently improves the performance of R-EDL, with the gap tending to widen as the value of λ increases. We speculate that as λ increases, the prediction becomes more dependent on the magnitude of the evidence rather than its proportion. Since \mathcal{L}_{kl} compresses the magnitude of the evidence, potentially reducing the information it carries, the negative impact of \mathcal{L}_{kl} on performance becomes more pronounced as λ grows.

Coefficient μ of regularization \mathcal{L}_{kl} . Acute readers may wonder how the coefficient of the KL-Div-minimizing regularization affects performances. In Table 8 we present the results on CIFAR-10 with varying values of the coefficient μ in EDL and Re-EDL, which clearly demonstrate that while this regularization can slightly improve classification accuracy with a carefully tuned coefficient, it generally leads to worse uncertainty estimation as the coefficient μ increases.

5.8 Ablation Study

Nonessential EDL settings. As summarized in Table 9, we evaluate the performance impact of relaxing individual or combined instances of the three nonessential EDL settings. These settings are denoted as follows: (1) $\lambda = 1$: the rigid setting of fixing prior weight to the number of classes, as

TABLE 12: Comparison of common evidence functions.

Evidence Functions	CIFAR10 Cls Acc	→SVHN OOD Detect	→CIFAR100 OOD Detect	Mean (six datasets) OOD Detect
ReLU	83.56±6.10	84.35±4.59	85.29±2.73	81.81±3.37
Softplus	90.13±0.25	89.94±1.40	88.31±0.16	85.46±1.41
Exp	89.81±0.18	83.72±2.55	87.16±0.30	82.39±2.03

discussed in Section 4.1; (2) \mathcal{L}_{var} : the variance-minimizing optimization loss, described in Section 4.2; (3) \mathcal{L}_{kl} : the KL-Div-minimizing regularization term, detailed in Section 4.3. Note that if \mathcal{L}_{kl} is retained, Re-EDL (row 8) reverts to the original R-EDL method (row 5). Furthermore, if both $\lambda = 1$ and \mathcal{L}_{var} are relaxed, R-EDL reverts to the traditional EDL method (row 1). As shown in rows 5, 6, and 7 of Table 9, retaining any of the original settings results in a decline in OOD detection performance. Specifically, when measured by the AUPR score for OOD detection averaged over six datasets, retaining any one of these settings reduces the performance of Re-EDL by 1.73%, 0.98%, and 0.34%, respectively. Additionally, a comparison between row 1 and row 8 reveals that when all three settings are relaxed, the performance of Re-EDL surpasses the baseline method by 1.65% on classification accuracy and 3.14% on OOD detection AUPR. Therefore, relaxing these settings is effective and their combined application further optimizes performance.

Components of essential EDL setting. In Section 4.4, we argue that the essential setting of EDL is replacing softmax with projected probability, which adds an extra parameter λ to class scores and employs an output activation function with a more gradual growth rate. As shown in Table 10, both modifications help preserve the useful magnitude information of logits, thereby enhancing uncertainty estimation.

Different loss formulations. Since we consider the use of projected probability from subjective logic to be the essential EDL setting, we also validate its effectiveness with the cross-entropy (CE) loss function, which is more commonly applied in classification tasks. As shown in Table 11, using CE to optimize the projected probability instead of the softmax probability also leads to enhanced uncertainty estimation and comparable classification accuracy.

Different evidence functions. In addition, we examine the effects of common evidence functions, including ReLU, Softplus, and Exp, as presented in Table 12. To ensure a fair comparison, the hyperparameter λ is consistently set to 1. Besides, the input to the Exp function is constrained within the range of -10 to 10 using the clamp function to prevent numerical overflow. Although Softplus is not the exclusive choice prescribed by subjective logic, it demon-

strates superior performance in both classification and OOD detection when compared to ReLU and Exp, supporting our analysis in Section 4.4. Specifically, the exponential growth rate characteristic of the Exp function transforms probability distributions into forms resembling one-hot encoding, whereas ReLU crudely truncates all negative logits, both of which result in substantial information loss.

5.9 More Experiment Results

Due to space limitations, please refer to Appendix C for additional results in the classical setting, few-shot setting, and ablation study, as well as visualizations of PR and ROC curves, and uncertainty distributions using various metrics.

6 CONCLUSION

Summary. We propose Re-EDL, a simplified yet more effective version of EDL, achieved by revisiting the essential and nonessential settings of the traditional method. Our analysis yields insights in two key aspects. On one hand, we identify the nonessential settings in traditional EDL, which include: (1) Fixing the prior weight parameter, which governs the balance between leveraging the proportion of evidence and its magnitude in deriving predictive scores, to the number of classes; (2) The empirical risk of EDL includes a variance-minimizing optimization term which encourages the Dirichlet PDF to approach a Dirac delta function, thereby heightening the risk of model overconfidence; (3) EDL’s structural risk adopts a KL-Div-minimizing regularization on non-target evidence, which extends its effect beyond the intended purpose and contradicts common sense, hindering uncertainty estimation in most cases. On the other hand, we identify the essential setting of EDL as the adoption of projected probability, which more effectively preserves the magnitude information of logits than the traditional softmax probability, thereby enhancing uncertainty estimation. Building on these insights, Re-EDL treats the prior weight as an adjustable hyperparameter instead of fixing it to the class number, and directly optimizes the expectation of the Dirichlet PDF, phasing out both the variance-minimizing optimization term and the regularization on non-target evidence. Comprehensive experimental evaluations underscore the efficacy of our method.

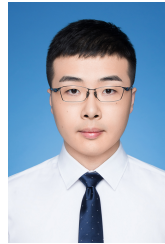
Deficiencies and Future directions. This paper can be extended along several directions below. (1) While the crucial role of the prior weight in balancing the trade-off between leveraging the evidence proportion and the magnitude has been elucidated, the underlying mechanism dictating its optimal value warrants further investigation. (2) The optimization objective of Re-EDL can be interpreted as optimizing the expected value of the constructed Dirichlet PDF. While principled and effective, it is somewhat coarse. Future work could explore optimization goals considering other statistical properties of Dirichlet PDFs. (3) Although Re-EDL deprecates the traditional KL-Div-minimizing regularization, experiments still validate its benefits in certain aspects. Exploring regularization that simultaneously enhances generalization and uncertainty estimation is worthwhile. In brief, we anticipate that Re-EDL, with its impressive simplicity, can establish a new baseline facilitating the single-forward-pass uncertainty quantification research.

REFERENCES

- [1] J. Choi, D. Chun, H. Kim, and H.-J. Lee, “Gaussian yolov3: An accurate and fast object detector using localization uncertainty for autonomous driving,” in *ICCV*, 2019, pp. 502–511.
- [2] M. Abdar, A. Khosravi, S. M. S. Islam, U. R. Acharya, and A. V. Vasilakos, “The need for quantification of uncertainty in artificial intelligence for clinical data analysis: increasing the level of trust in the decision-making process,” *IEEE Systems, Man, and Cybernetics Magazine*, vol. 8, no. 3, pp. 28–40, 2022.
- [3] C. Blundell, J. Cornebise, K. Kavukcuoglu, and D. Wierstra, “Weight uncertainty in neural network,” in *ICML*. PMLR, 2015, pp. 1613–1622.
- [4] M. Dusenberry, G. Jerfel, Y. Wen, Y. Ma, J. Snoek, K. Heller, B. Lakshminarayanan, and D. Tran, “Efficient and scalable bayesian neural nets with rank-1 factors,” in *ICML*. PMLR, 2020, pp. 2782–2792.
- [5] Y. Gal and Z. Ghahramani, “Dropout as a bayesian approximation: Representing model uncertainty in deep learning,” in *ICML*. PMLR, 2016, pp. 1050–1059.
- [6] B. Lakshminarayanan, A. Pritzel, and C. Blundell, “Simple and scalable predictive uncertainty estimation using deep ensembles,” *NeurIPS*, vol. 30, 2017.
- [7] Y. Wen, D. Tran, and J. Ba, “Batchensemble: an alternative approach to efficient ensemble and lifelong learning,” *arXiv preprint arXiv:2002.06715*, 2020.
- [8] R. Egele, R. Maulik, K. Raghavan, B. Lusch, I. Guyon, and P. Balaprakash, “Autodeuq: Automated deep ensemble with uncertainty quantification,” in *ICPR*. IEEE, 2022, pp. 1908–1914.
- [9] M. Sensoy, L. Kaplan, and M. Kandemir, “Evidential deep learning to quantify classification uncertainty,” *NeurIPS*, vol. 31, 2018.
- [10] A. Amini, W. Schwarting, A. Soleimany, and D. Rus, “Deep evidential regression,” *NeurIPS*, vol. 33, pp. 14 927–14 937, 2020.
- [11] W. Bao, Q. Yu, and Y. Kong, “Evidential deep learning for open set action recognition,” in *ICCV*, 2021, pp. 13 349–13 358.
- [12] Y. Qin, D. Peng, X. Peng, X. Wang, and P. Hu, “Deep evidential learning with noisy correspondence for cross-modal retrieval,” in *ACM MM*, 2022, pp. 4948–4956.
- [13] M. Chen, J. Gao, S. Yang, and C. Xu, “Dual-evidential learning for weakly-supervised temporal action localization,” in *ECCV*. Springer, 2022, pp. 192–208.
- [14] D. Oh and B. Shin, “Improving evidential deep learning via multi-task learning,” in *AAAI*, vol. 36, no. 7, 2022, pp. 7895–7903.
- [15] S. Sun, S. Zhi, J. Heikkilä, and L. Liu, “Evidential uncertainty and diversity guided active learning for scene graph generation,” in *ICLR*, 2022.
- [16] Y. Park, W. Choi, S. Kim, D.-J. Han, and J. Moon, “Active learning for object detection with evidential deep learning and hierarchical uncertainty aggregation,” in *ICLR*, 2022.
- [17] H. Sapkota and Q. Yu, “Adaptive robust evidential optimization for open set detection from imbalanced data,” in *ICLR*, 2022.
- [18] J. Gao, M. Chen, and C. Xu, “Collecting cross-modal presence-absence evidence for weakly-supervised audio-visual event perception,” in *CVPR*, 2023, pp. 18 827–18 836.
- [19] A. Josang, “A logic for uncertain probabilities,” *International Journal of Uncertainty, Fuzziness and Knowledge-Based Systems*, vol. 9, no. 03, pp. 279–311, 2001.
- [20] —, *Subjective logic*. Springer, 2016, vol. 3.
- [21] M. Chen, J. Gao, and C. Xu, “R-edl: Relaxing nonessential settings of evidential deep learning,” in *ICLR*, 2024.
- [22] M. Sensoy, L. Kaplan, F. Cerutti, and M. Saleki, “Uncertainty-aware deep classifiers using generative models,” in *AAAI*, vol. 34, no. 04, 2020, pp. 5620–5627.
- [23] C. Doersch, “Tutorial on variational autoencoders,” *arXiv preprint arXiv:1606.05908*, 2016.
- [24] Y. Hu, Y. Ou, X. Zhao, J.-H. Cho, and F. Chen, “Multidimensional uncertainty-aware evidential neural networks,” in *AAAI*, vol. 35, no. 9, 2021, pp. 7815–7822.
- [25] A. Nagahama, “Learning and predicting the unknown class using evidential deep learning,” *Scientific Reports*, vol. 13, no. 1, p. 14904, 2023.
- [26] X. Zhao, Y. Ou, L. Kaplan, F. Chen, and J.-H. Cho, “Quantifying classification uncertainty using regularized evidential neural networks,” *arXiv preprint arXiv:1910.06864*, 2019.
- [27] M. Shen, Y. Bu, P. Sattigeri, S. Ghosh, S. Das, and G. Wornell, “Post-hoc uncertainty learning using a dirichlet meta-model,” in *AAAI*, vol. 37, no. 8, 2023, pp. 9772–9781.

- [28] D. S. Pandey and Q. Yu, "Learn to accumulate evidence from all training samples: theory and practice," in *ICML*. PMLR, 2023, pp. 26 963–26 989.
- [29] D. Deng, G. Chen, Y. Yu, F. Liu, and P.-A. Heng, "Uncertainty estimation by fisher information-based evidential deep learning," *arXiv preprint arXiv:2303.02045*, 2023.
- [30] C. Li, K. Li, Y. Ou, L. M. Kaplan, A. Jøsang, J.-H. Cho, D. H. Jeong, and F. Chen, "Hyper evidential deep learning to quantify composite classification uncertainty," 2023.
- [31] M. Kandemir, A. Akgül, M. Hausmann, and G. Unal, "Evidential turing processes," in *International Conference on Learning Representations*, 2022.
- [32] F. C. Ghesu, B. Georgescu, E. Gibson, S. Guendel, M. K. Kalra, R. Singh, S. R. Digumarthy, S. Grbic, and D. Comaniciu, "Quantifying and leveraging classification uncertainty for chest radiograph assessment," in *MICCAI*, 2019.
- [33] F. Ji, W. Zhao, Q. Wang, W. J. Emery, R. Peng, Y. Man, G. Wang, and K. Jia, "Spectral-spatial evidential learning network for open-set hyperspectral image classification," *IEEE Transactions on Geoscience and Remote Sensing*, 2024.
- [34] R. Shi, L. Duan, T. Huang, and T. Jiang, "Evidential uncertainty-guided mitochondria segmentation for 3d em images," in *AAAI*, 2024.
- [35] C. Wang, X. Wang, J. Zhang, L. Zhang, X. Bai, X. Ning, J. Zhou, and E. Hancock, "Uncertainty estimation for stereo matching based on evidential deep learning," *Pattern Recognition*, vol. 124, p. 108498, 2022.
- [36] J. Lou, W. Liu, Z. Chen, F. Liu, and J. Cheng, "Elfnet: Evidential local-global fusion for stereo matching," in *ICCV*, 2023.
- [37] H. Zhang, Y. Liu, Y. Wang, L. Wang, and Y. Qiao, "Learning discriminative feature representation for open set action recognition," in *ACM MM*, 2023.
- [38] C. Zhao, D. Du, A. Hoogs, and C. Funk, "Open set action recognition via multi-label evidential learning," in *CVPR*, 2023.
- [39] Y. Zhu, W. Bao, and Q. Yu, "Towards open set video anomaly detection," in *ECCV*, 2022.
- [40] W. Bao, Q. Yu, and Y. Kong, "Opental: Towards open set temporal action localization," in *CVPR*, 2022.
- [41] C. Sun, Y. Jia, and Y. Wu, "Evidential reasoning for video anomaly detection," in *ACM MM*, 2022.
- [42] M. Chen, J. Gao, and C. Xu, "Uncertainty-aware dual-evidential learning for weakly-supervised temporal action localization," *IEEE transactions on pattern analysis and machine intelligence*, 2023.
- [43] Z. Zhang, M. Hu, S. Zhao, M. Huang, H. Wang, L. Liu, Z. Zhang, Z. Liu, and B. Wu, "E-ner: Evidential deep learning for trustworthy named entity recognition," *arXiv:2305.17854*, 2023.
- [44] J. Ren, L. Jiang, H. Peng, Z. Liu, J. Wu, and S. Y. Philip, "Evidential temporal-aware graph-based social event detection via Dempster-Shafer theory," in *2022 IEEE International Conference on Web Services (ICWS)*. IEEE, 2022, pp. 331–336.
- [45] J. Ren, H. Peng, L. Jiang, Z. Liu, J. Wu, Z. Yu, and S. Y. Philip, "Uncertainty-guided boundary learning for imbalanced social event detection," *IEEE Transactions on Knowledge and Data Engineering*, 2023.
- [46] S. Li, X. Xu, Y. Yang, F. Shen, Y. Mo, Y. Li, and H. T. Shen, "Dcel: Deep cross-modal evidential learning for text-based person retrieval," in *ACM MM*, 2023, pp. 6292–6300.
- [47] Z. Shao, W. Dou, and Y. Pan, "Dual-level deep evidential fusion: Integrating multimodal information for enhanced reliable decision-making in deep learning," *Information Fusion*, vol. 103, p. 102113, 2024.
- [48] H. Li, J. Song, L. Gao, X. Zhu, and H. Shen, "Prototype-based aleatoric uncertainty quantification for cross-modal retrieval," *NeurIPS*, vol. 36, 2024.
- [49] A. R. Tan, S. Urata, S. Goldman, J. C. Dietschreit, and R. Gómez-Bombarelli, "Single-model uncertainty quantification in neural network potentials does not consistently outperform model ensembles," *npj Computational Materials*, vol. 9, no. 1, p. 225, 2023.
- [50] L. I. Vazquez-Salazar, S. Käser, and M. Meuwly, "Outlier-detection for reactive machine learned potential energy surfaces," *arXiv:2402.17686*, 2024.
- [51] W. Shi, X. Zhao, F. Chen, and Q. Yu, "Multifaceted uncertainty estimation for label-efficient deep learning," *NeurIPS*, vol. 33, pp. 17 247–17 257, 2020.
- [52] L. Chen, Y. Lou, J. He, T. Bai, and M. Deng, "Evidential neighborhood contrastive learning for universal domain adaptation," in *AAAI*, vol. 36, no. 6, 2022, pp. 6258–6267.
- [53] E. Aguilar, B. Raducanu, P. Radeva, and J. Van de Weijer, "Continual evidential deep learning for out-of-distribution detection," in *ICCV*, 2023, pp. 3444–3454.
- [54] J. Pei, A. Men, Y. Liu, X. Zhuang, and Q. Chen, "Evidential multi-source-free unsupervised domain adaptation," *IEEE Transactions on Pattern Analysis and Machine Intelligence*, 2024.
- [55] W. Zhang, Z. Lv, H. Zhou, J.-W. Liu, J. Li, M. Li, Y. Li, D. Zhang, Y. Zhuang, and S. Tang, "Revisiting the domain shift and sample uncertainty in multi-source active domain transfer," in *CVPR*, 2024, pp. 16 751–16 761.
- [56] H. Yang, C. Chen, Y. Chen, H. C. Yip, and D. Qi, "Uncertainty estimation for safety-critical scene segmentation via fine-grained reward maximization," *NeurIPS*, vol. 36, pp. 36 238–36 249, 2023.
- [57] D. Wang, D. S. Pandey, K. P. Neupane, Z. Yu, E. Zheng, Z. Zheng, and Q. Yu, "Deep temporal sets with evidential reinforced attentions for unique behavioral pattern discovery," in *ICML*. PMLR, 2023, pp. 36 205–36 223.
- [58] J. Gao, M. Chen, and C. Xu, "Vectorized evidential learning for weakly-supervised temporal action localization," *IEEE Transactions on Pattern Analysis and Machine Intelligence*, 2023.
- [59] M. Chen, J. Gao, and C. Xu, "Cascade evidential learning for open-world weakly-supervised temporal action localization," in *CVPR*, 2023, pp. 14 741–14 750.
- [60] B. Su, H. Zhang, and Z. Zhou, "Hsic-based moving weight averaging for few-shot open-set object detection," in *ACM MM*, 2023, pp. 5358–5369.
- [61] A. P. Soleimany, A. Amini, S. Goldman, D. Rus, S. N. Bhatia, and C. W. Coley, "Evidential deep learning for guided molecular property prediction and discovery," *ACS central science*, vol. 7, no. 8, pp. 1356–1367, 2021.
- [62] N. Meinert and A. Lavin, "Multivariate deep evidential regression," *arXiv preprint arXiv:2104.06135*, 2021.
- [63] H. Ma, Z. Han, C. Zhang, H. Fu, J. T. Zhou, and Q. Hu, "Trustworthy multimodal regression with mixture of normal-inverse gamma distributions," *NeurIPS*, vol. 34, pp. 6881–6893, 2021.
- [64] N. Meinert, J. Gawlikowski, and A. Lavin, "The unreasonable effectiveness of deep evidential regression," in *AAAI*, vol. 37, no. 8, 2023, pp. 9134–9142.
- [65] K. Ye, T. Chen, H. Wei, and L. Zhan, "Uncertainty regularized evidential regression," *arXiv preprint arXiv:2401.01484*, 2024.
- [66] Y. Wu, B. Shi, B. Dong, Q. Zheng, and H. Wei, "The evidence contraction issue in deep evidential regression: Discussion and solution," in *AAAI*, vol. 38, no. 19, 2024, pp. 21 726–21 734.
- [67] R. Duan, B. Caffo, H. X. Bai, H. I. Sair, and C. Jones, "Evidential uncertainty quantification: A variance-based perspective," in *Proceedings of the IEEE/CVF Winter Conference on Applications of Computer Vision*, 2024, pp. 2132–2141.
- [68] D. S. Pandey and Q. Yu, "Evidential conditional neural processes," in *AAAI*, vol. 37, no. 8, 2023, pp. 9389–9397.
- [69] H. Ritter, A. Botev, and D. Barber, "A scalable laplace approximation for neural networks," in *6th International Conference on Learning Representations, ICLR 2018-Conference Track Proceedings*, vol. 6. International Conference on Representation Learning, 2018.
- [70] P. Izmailov, S. Vikram, M. D. Hoffman, and A. G. G. Wilson, "What are bayesian neural network posteriors really like?" in *ICML*. PMLR, 2021, pp. 4629–4640.
- [71] J. Van Amersfoort, L. Smith, Y. W. Teh, and Y. Gal, "Uncertainty estimation using a single deep deterministic neural network," in *ICML*. PMLR, 2020, pp. 9690–9700.
- [72] J. Liu, Z. Lin, S. Padhy, D. Tran, T. Bedrax Weiss, and B. Lakshminarayanan, "Simple and principled uncertainty estimation with deterministic deep learning via distance awareness," *NeurIPS*, vol. 33, pp. 7498–7512, 2020.
- [73] A. Malinin and M. Gales, "Predictive uncertainty estimation via prior networks," *NeurIPS*, vol. 31, 2018.
- [74] —, "Reverse kl-divergence training of prior networks: Improved uncertainty and adversarial robustness," *NeurIPS*, vol. 32, 2019.
- [75] B. Charpentier, D. Zügner, and S. Günnemann, "Posterior network: Uncertainty estimation without ood samples via density-based pseudo-counts," *NeurIPS*, vol. 33, pp. 1356–1367, 2020.
- [76] B. Charpentier, O. Borchert, D. Zügner, S. Geisler, and S. Günnemann, "Natural posterior network: Deep bayesian uncertainty for exponential family distributions," in *ICLR*, 2022.
- [77] Z. Han, C. Zhang, H. Fu, and J. T. Zhou, "Trusted multi-view classification with dynamic evidential fusion," *IEEE transactions on pattern analysis and machine intelligence*, vol. 45, no. 2, pp. 2551–2566, 2022.

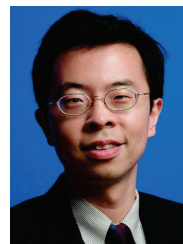
- [78] M. Xie, Z. Han, C. Zhang, Y. Bai, and Q. Hu, "Exploring and exploiting uncertainty for incomplete multi-view classification," in *CVPR*, 2023, pp. 19 873–19 882.
- [79] L. Fan, B. Liu, H. Li, Y. Wu, and G. Hua, "Flexible visual recognition by evidential modeling of confusion and ignorance," in *ICCV*, 2023, pp. 1338–1347.
- [80] H. Sapkota and Q. Yu, "Adaptive robust evidential optimization for open set detection from imbalanced data," in *ICLR*, 2023.
- [81] D. S. Pandey and Q. Yu, "Multidimensional belief quantification for label-efficient meta-learning," in *CVPR*, 2022, pp. 14 391–14 400.
- [82] A. Bendale and T. E. Boult, "Towards open set deep networks," in *Proceedings of the IEEE conference on computer vision and pattern recognition*, 2016, pp. 1563–1572.
- [83] R. Krishnan, M. Subedar, and O. Tickoo, "Bar: Bayesian activity recognition using variational inference," *arXiv preprint arXiv:1811.03305*, 2018.
- [84] G. Chen, L. Qiao, Y. Shi, P. Peng, J. Li, T. Huang, S. Pu, and Y. Tian, "Learning open set network with discriminative reciprocal points," in *Computer Vision–ECCV 2020: 16th European Conference, Glasgow, UK, August 23–28, 2020, Proceedings, Part III 16*. Springer, 2020, pp. 507–522.
- [85] Y. Netzer, T. Wang, A. Coates, A. Bissacco, B. Wu, and A. Ng, "The street view house numbers (svhn) dataset," Technical report, Accessed 2016-08-01.[Online], Tech. Rep., 2018.
- [86] A. Krizhevsky, G. Hinton *et al.*, "Learning multiple layers of features from tiny images," 2009.
- [87] J. Stallkamp, M. Schlipsing, J. Salmen, and C. Igel, "Man vs. computer: Benchmarking machine learning algorithms for traffic sign recognition," *Neural networks*, vol. 32, pp. 323–332, 2012.
- [88] G. B. Huang, M. Mattar, T. Berg, and E. Learned-Miller, "Labeled faces in the wild: A database for studying face recognition in unconstrained environments," in *Workshop on faces in Real-Life Images: detection, alignment, and recognition*, 2008.
- [89] B. Zhou, A. Lapedriza, A. Khosla, A. Oliva, and A. Torralba, "Places: A 10 million image database for scene recognition," *IEEE Transactions on Pattern Analysis and Machine Intelligence*, 2017.
- [90] L. Bossard, M. Guillaumin, and L. Van Gool, "Food-101 – mining discriminative components with random forests," in *ECCV*, 2014.
- [91] H. Xiao, K. Rasul, and R. Vollgraf, "Fashion-mnist: a novel image dataset for benchmarking machine learning algorithms," *arXiv preprint arXiv:1708.07747*, 2017.
- [92] T. Clanuwat, M. Bober-Irizar, A. Kitamoto, A. Lamb, K. Yamamoto, and D. Ha, "Deep learning for classical japanese literature," *arXiv preprint arXiv:1812.01718*, 2018.
- [93] S. Yang, L. Liu, and M. Xu, "Free lunch for few-shot learning: Distribution calibration," *arXiv preprint arXiv:2101.06395*, 2021.
- [94] O. Vinyals, C. Blundell, T. Lillicrap, D. Wierstra *et al.*, "Matching networks for one shot learning," *NeurIPS*, vol. 29, 2016.
- [95] C. Wah, S. Branson, P. Welinder, P. Perona, and S. Belongie, "The caltech-ucsd birds-200-2011 dataset," 2011.
- [96] K. Soomro, A. R. Zamir, and M. Shah, "Ucf101: A dataset of 101 human actions classes from videos in the wild," *arXiv preprint arXiv:1212.0402*, 2012.
- [97] H. Kuehne, H. Jhuang, E. Garrote, T. Poggio, and T. Serre, "Hmdb: a large video database for human motion recognition," in *ICCV*. IEEE, 2011, pp. 2556–2563.
- [98] M. Monfort, B. Pan, K. Ramakrishnan, A. Andonian, B. A. McMara, A. Lascelles, Q. Fan, D. Gutfreund, R. S. Feris, and A. Oliva, "Multi-moments in time: Learning and interpreting models for multi-action video understanding," *IEEE Transactions on Pattern Analysis and Machine Intelligence*, vol. 44, no. 12, pp. 9434–9445, 2021.
- [99] J. Gao, T. Zhang, and C. Xu, "Learning to model relationships for zero-shot video classification," *IEEE transactions on pattern analysis and machine intelligence*, vol. 43, no. 10, pp. 3476–3491, 2020.
- [100] D. A. McAllester, "Some pac-bayesian theorems," in *Proceedings of the eleventh annual conference on Computational learning theory*, 1998, pp. 230–234.
- [101] G. Shafer, *A mathematical theory of evidence*. Princeton university press, 1976, vol. 42.
- [102] A. P. Dempster, "Upper and lower probabilities induced by a multivalued mapping," in *Classic works of the Dempster-Shafer theory of belief functions*. Springer, 2008, pp. 57–72.
- [103] P. Walley, "Inferences from multinomial data: learning about a bag of marbles," *Journal of the Royal Statistical Society Series B: Statistical Methodology*, vol. 58, no. 1, pp. 3–34, 1996.
- [104] P. Hájek, *Metamathematics of fuzzy logic*. Springer Science & Business Media, 2013, vol. 4.
- [105] A. Jøsang, X. Luo, and X. Chen, "Continuous ratings in discrete bayesian reputation systems," in *Trust Management II: Proceedings of IFIP TM 2008: Joint iTrust and PST Conferences on Privacy, Trust Management and Security, June 18-20, 2008, Trondheim, Norway 2*. Springer, 2008, pp. 151–166.
- [106] M. Fitting, "Kleene's three valued logics and their children," *Fundamenta informaticae*, vol. 20, no. 1, 2, 3, pp. 113–131, 1994.
- [107] Y. LeCun, "The mnist database of handwritten digits," <http://yann.lecun.com/exdb/mnist/>, 1998.
- [108] C. Guo, G. Pleiss, Y. Sun, and K. Q. Weinberger, "On calibration of modern neural networks," in *ICML*. PMLR, 2017, pp. 1321–1330.



Mengyuan Chen is currently a Ph.D. candidate at the State Key Laboratory of Multimodal Artificial Intelligence Systems, Institute of Automation, Chinese Academy of Sciences, Beijing, China. His research interests include video understanding and uncertainty estimation.



Junyu Gao is an Associate Professor at the Institute of Automation, Chinese Academy of Sciences, Beijing, China. His research interests include computer vision and embodied AI, especially video understanding, vision-and-language navigation, and cross-modal learning.



Changsheng Xu (M'97–SM'99–F'14) is a Professor in the State Key Laboratory of Multimodal Artificial Intelligence Systems (MAIS), Institute of Automation, Chinese Academy of Sciences. His research interests include multimedia content analysis/indexing/retrieval, pattern recognition and computer vision. He has held 50 granted/pending patents and published over 400 refereed research papers in these areas. He is IEEE Fellow, IAPR Fellow and ACM Distinguished Scientist.

APPENDIX A

PROOF AND DERIVATION

This section provides the proof of Theorem 1 and the derivation of optimization objectives of EDL.

A.1 Proof of Theorem 1

Theorem 1 (Bijection between subjective opinions and Dirichlet PDFs). Let X be a random variable defined in domain \mathbb{X} , and $\omega_X = (\mathbf{b}_X, u_X, \mathbf{a}_X)$ be a subjective opinion. \mathbf{p}_X is a probability distribution over \mathbb{X} , and a Dirichlet PDF with the concentration parameter α_X is denoted by $\text{Dir}(\mathbf{p}_X, \alpha_X)$, where $\alpha_X(x) \geq 0$, and $\mathbf{p}_X(x) \neq 0$ if $\alpha_X(x) < 1$. Then, given the base rate \mathbf{a}_X , there exists a bijection F between the opinion ω_X and the Dirichlet PDF $\text{Dir}(\mathbf{p}_X, \alpha_X)$:

$$F : \omega_X = (\mathbf{b}_X, u_X, \mathbf{a}_X) \mapsto \text{Dir}(\mathbf{p}_X, \alpha_X) = \frac{\Gamma(\sum_{x \in \mathbb{X}} \alpha_X(x))}{\prod_{x \in \mathbb{X}} \Gamma(\alpha_X(x))} \prod_{x \in \mathbb{X}} \mathbf{p}_X(x)^{\alpha_X(x)-1}, \quad (19)$$

where Γ denotes the Gamma function, α_X satisfies the following identity that

$$\alpha_X(x) = \frac{\mathbf{b}_X(x)W}{u_X} + \mathbf{a}_X(x)W, \quad (20)$$

$W \in \mathbb{R}_+$ is a given scalar representing a non-informative prior weight.

Proof. The proof of the bijection will be performed in two steps. First, we will prove a Dirichlet distribution $\text{Dir}(\mathbf{p}_X, \alpha_X)$ is uniquely specified by its parameters α_X , aka there exists a bijective mapping between $\text{Dir}(\mathbf{p}_X, \alpha_X)$ and α_X . Then, we will prove the bijection between the Dirichlet parameters α_X and the subjective opinion ω_X . Therefore, the bijection between ω_X and $\text{Dir}(\mathbf{p}_X, \alpha_X)$ can be established due to the transitivity of bijection.

Step 1: To prove the mapping $F_1 : \alpha_X \mapsto \text{Dir}(\mathbf{p}_X, \alpha_X)$ is bijective, we will prove it is both injective and surjective. The surjective property is obvious due to the mapping form. We use proof by contradiction to verify the injectivity as follows.

Assuming that there exists two Dirichlet distributions over the random variable X , which are parameterized by two different concentration parameter vectors α_X and $\tilde{\alpha}_X$ respectively, sharing exactly the same probability density function, i.e., there exists $x \in \mathbb{X}$, $\alpha_X(x) \neq \tilde{\alpha}_X(x)$, and for any $x \in \mathbb{X}$ and any $\mathbf{p}_X \in \mathcal{S}_{|\mathbb{X}|}$, the equation

$$\begin{aligned} & \frac{\Gamma(\sum_{x \in \mathbb{X}} \alpha_X(x))}{\prod_{x \in \mathbb{X}} \Gamma(\alpha_X(x))} \prod_{x \in \mathbb{X}} \mathbf{p}_X(x)^{\alpha_X(x)-1} \\ &= \frac{\Gamma(\sum_{x \in \mathbb{X}} \tilde{\alpha}_X(x))}{\prod_{x \in \mathbb{X}} \Gamma(\tilde{\alpha}_X(x))} \prod_{x \in \mathbb{X}} \mathbf{p}_X(x)^{\tilde{\alpha}_X(x)-1}, \end{aligned} \quad (21)$$

holds, where $\mathcal{S}_{|\mathbb{X}|}$ is a $|\mathbb{X}|$ -dimensional unit simplex. Taking the logarithm of both sides, we have

$$\begin{aligned} & -\log(B(\alpha_X(x))) + \sum_{x \in \mathbb{X}} (\alpha_X(x) - 1) \log(\mathbf{p}_X(x)) \\ &= -\log(B(\tilde{\alpha}_X(x))) + \sum_{x \in \mathbb{X}} (\tilde{\alpha}_X(x) - 1) \log(\mathbf{p}_X(x)), \end{aligned} \quad (22)$$

where B denotes a $|\mathbb{X}|$ -dimensional beta function. Therefore, we have the following equation

$$\sum_{x \in \mathbb{X}} (\alpha_X(x) - \tilde{\alpha}_X(x)) \log(\mathbf{p}_X(x)) = \log\left(\frac{B(\alpha_X(x))}{B(\tilde{\alpha}_X(x))}\right), \quad (23)$$

for any $\mathbf{p}_X \in \mathcal{S}_{|\mathbb{X}|}$. Since the above equation holds for any probability distribution \mathbf{p}_X , we have

$$\sum_{x \in \mathbb{X}} (\alpha_X(x) - \tilde{\alpha}_X(x)) \log(\mathbf{p}_X(x) - \mathbf{p}'_X(x)) = 0, \quad (24)$$

for any $\mathbf{p}_X, \mathbf{p}'_X \in \mathcal{S}_{|\mathbb{X}|}$. The above equation can be regarded as a homogenous linear equation with $\alpha_X(x) - \tilde{\alpha}_X(x)$ as variables and $\log(\mathbf{p}_X(x) - \mathbf{p}'_X(x))$ as parameters. Due to the arbitrariness of \mathbf{p}_X and \mathbf{p}'_X , and the property of homogeneous systems of linear equations, we know that Eqn. 24 only has a particular solution, i.e., $\alpha_X(x) - \tilde{\alpha}_X(x) = 0$ for any $x \in \mathbb{X}$, which violates our assumption.

Therefore, F_1 is injective and surjective, thus bijective.

Step 2: To prove the bijection between ω_X and α_X , we also need to prove the mapping $F_2 : \omega_X \mapsto \alpha_X$ is both injective and surjective. Since the base rate \mathbf{a}_X and the non-informative prior weight W in Eqn. 20 are given, F_2 can be simplified to $(\mathbf{b}_X, u_X) \mapsto \alpha_X$ with the formulation:

$$\alpha_X(x) = \frac{\mathbf{b}_X(x)}{u_X}, \quad \forall x \in \mathbb{X}. \quad (25)$$

First, we use proof by contradiction to verify the injectivity. Assuming that there exists two different sets of belief mass and uncertainty mass which corresponds to the same set of Dirichlet concentration parameters, aka there exists $(\mathbf{b}_X, u_X), (\tilde{\mathbf{b}}_X, \tilde{u}_X), \alpha_X$, which satisfies

$$\alpha_X(x) = \frac{\mathbf{b}_X(x)}{u_X} = \frac{\tilde{\mathbf{b}}_X(x)}{\tilde{u}_X}, \quad \forall x \in \mathbb{X}, \quad (26)$$

and $\exists x \in \mathbb{X}$, $\mathbf{b}_X(x) \neq \tilde{\mathbf{b}}_X(x)$, or $u_X \neq \tilde{u}_X$. We take the summation of Eqn. 26 across all possible values of $x \in \mathbb{X}$ and utilize the additivity requirement $\sum_{x \in \mathbb{X}} \mathbf{b}_X(x) + u_X = 1$, then we will have

$$\sum_{x \in \mathbb{X}} \alpha_X(x) = \frac{1 - u_X}{u_X} = \frac{1 - \tilde{u}_X}{\tilde{u}_X}. \quad (27)$$

Thus we reach $u_X = \tilde{u}_X$ and after using the relationship in Eqn. 26, we will have $\mathbf{b}_X(x) = \tilde{\mathbf{b}}_X(x), \forall x \in \mathbb{X}$. Thereafter, our assumption is violated and thus F_2 is injective.

Second, we prove F_2 is surjective, aka for any Dirichlet parameter set α_X , there exists a set of (\mathbf{b}_X, u_X) satisfying Eqn. 25. By summing Eqn. 25 over all values of $x \in \mathbb{X}$, we obtain the following formulation:

$$S_X = \frac{1 - u_X}{u_X}, \quad (28)$$

where $S_X = \sum_{x \in \mathbb{X}} \alpha_X(x)$. By reorganization and substituting u_X into Eqn. 25, we have

$$u_X = \frac{1}{S_X + 1}, \quad \mathbf{b}_X(x) = \frac{\alpha_X(x)}{S_X + 1}, \quad (29)$$

which satisfy all the requirements. Therefore, the mapping F_2 is surjective.

Finally, since F_1 and F_2 are both bijective, $F = F_1 \circ F_2$ is also bijective. \square

Moreover, in cases of no prior information available, we generally set the base rate $\alpha_X(x)$ as uniform distribution, i.e., $\alpha_X(x) = \frac{1}{|\mathbb{X}|}$, $\forall x \in \mathbb{X}$, and Eqn. 20 can be reorganized as

$$\alpha_X(x) = \left(\frac{b_X(x)}{u_X} + \frac{1}{|\mathbb{X}|} \right) W, \quad \forall x \in \mathbb{X}, \quad (30)$$

or equivalently as

$$b_X(x) = \frac{\alpha_X(x) - W/|\mathbb{X}|}{\sum_{x' \in \mathbb{X}} \alpha_X(x')}, \quad u_X = \frac{W}{\sum_{x \in \mathbb{X}} \alpha_X(x)}, \quad (31)$$

by utilizing the additivity condition $\sum_{x \in \mathbb{X}} b_X(x) + u_X = 1$.

Besides, it is noteworthy that comprehensive elaborations on the concepts within the Subjective Logic theory are available in [19], [20].

A.2 Derivation of Optimization Objectives in EDL

As aforementioned in Section 3.2, to perform model optimization, EDL integrates the conventional MSE loss function over the class probability p_X which is assumed to follow the Dirichlet PDF specified in the bijection, thus derives the optimization objective as

$$\begin{aligned} \mathcal{L}_{\text{edl}} &= \sum_{(\mathbf{z}, \mathbf{y}) \in \mathcal{D}} \mathbb{E}_{\mathbf{p}_X \sim \text{Dir}(\mathbf{p}_X, \alpha_X)} [\|\mathbf{y} - \mathbf{p}_X\|_2^2] \\ &= \sum_{(\mathbf{z}, \mathbf{y}) \in \mathcal{D}} \mathbb{E}_{\mathbf{p}_X \sim \text{Dir}(\mathbf{p}_X, \alpha_X)} \sum_{x \in \mathbb{X}} (\mathbf{y}_x^2 - 2\mathbf{y}_x \mathbf{p}_X(x) + \mathbf{p}_X(x)^2) \\ &= \sum_{(\mathbf{z}, \mathbf{y}) \in \mathcal{D}} \sum_{x \in \mathbb{X}} (\mathbf{y}_x^2 - 2\mathbf{y}_x \mathbb{E}_{\mathbf{p}_X \sim \text{Dir}(\mathbf{p}_X, \alpha_X)} [\mathbf{p}_X(x)] \\ &\quad + \mathbb{E}_{\mathbf{p}_X \sim \text{Dir}(\mathbf{p}_X, \alpha_X)} [\mathbf{p}_X(x)^2]). \end{aligned} \quad (32)$$

Using the identity $\mathbb{E}[x^2] = \mathbb{E}[x]^2 + \text{Var}[x]$, we know that

$$\begin{aligned} \mathcal{L}_{\text{edl}} &= \sum_{(\mathbf{z}, \mathbf{y}) \in \mathcal{D}} \sum_{x \in \mathbb{X}} (\mathbf{y}_x - \mathbb{E}_{\mathbf{p}_X \sim \text{Dir}(\mathbf{p}_X, \alpha_X)} [\mathbf{p}_X(x)])^2 \\ &\quad + \text{Var}_{\mathbf{p}_X \sim \text{Dir}(\mathbf{p}_X, \alpha_X)} [\mathbf{p}_X(x)]. \end{aligned} \quad (33)$$

Since the Dirichlet distribution has the following properties:

$$\begin{aligned} \mathbb{E}[\mathbf{p}_X(x)] &= \frac{\alpha_X(x)}{S_X}, \\ \text{Var}[\mathbf{p}_X(x)] &= \frac{\alpha_X(x)(S_X - \alpha_X(x))}{S_X^2(S_X + 1)}, \end{aligned} \quad (34)$$

where $S_X = \sum_{i=1}^C \alpha_X(x)$, we can explicitly express \mathcal{L}_{edl} by $\alpha_X(x)$ and S_X as

$$\mathcal{L}_{\text{edl}} = \sum_{(\mathbf{z}, \mathbf{y}) \in \mathcal{D}} \sum_{x \in \mathbb{X}} \left(\mathbf{y}_x - \frac{\alpha_X(x)}{S_X} \right)^2 + \frac{\alpha_X(x)(S_X - \alpha_X(x))}{S_X^2(S_X + 1)}. \quad (35)$$

Furthermore, EDL introduces an auxiliary regularization term to suppress the evidence of non-target classes by minimizing the Kullback-Leibler (KL) divergence between a modified Dirichlet distribution and a uniform distribution. This regularization term has demonstrated promising empirical results and has been elucidated by [29] using the PAC-Bayesian theory [100]. Specifically, the regularization term has the following form:

$$\begin{aligned} \mathcal{L}_{\text{kl}} &= \frac{1}{|\mathcal{D}|} \sum_{(\mathbf{z}, \mathbf{y}) \in \mathcal{D}} \text{KL}(\text{Dir}(\mathbf{p}_X, \tilde{\alpha}_X), \text{Dir}(\mathbf{p}_X, \mathbf{1})) \\ &= \frac{1}{|\mathcal{D}|} \sum_{(\mathbf{z}, \mathbf{y}) \in \mathcal{D}} \left(\log \frac{\Gamma(\tilde{S}_X)}{\Gamma(C) \prod_{x \in \mathbb{X}} \Gamma(\tilde{\alpha}_X(x))} + \right. \\ &\quad \left. \sum_{x \in \mathbb{X}} (\tilde{\alpha}_X(x) - 1) (\psi(\tilde{\alpha}_X(x)) - \psi(\tilde{S}_X)) \right), \end{aligned} \quad (36)$$

where $\mathbf{1}$ denotes a C -dimensional ones vector, Γ denotes the Gamma function, and ψ denotes the digamma function. $\tilde{\alpha}_X = \mathbf{y} + (\mathbf{1} - \mathbf{y}) \odot \alpha_X$ a modified Dirichlet parameter vector whose value of the target class has been set to 1, \odot denotes Hadamard product, and $\tilde{S}_X = \sum_{x \in \mathbb{X}} \tilde{\alpha}_X(x)$.

Next, we provide the calculation process of the modified KL-divergence-based regularization term $\mathcal{L}_{\text{kl}}(\lambda)$ in Eqn. 16:

$$\begin{aligned} &\text{KL}(\text{Dir}(\mathbf{P}_X, \alpha_X^\lambda), \text{Dir}(\mathbf{P}_X, \lambda \cdot \mathbf{1})) \\ &= \int_{\mathbf{P}_X \in \mathcal{N}_C} \text{Dir}(\mathbf{P}_X, \alpha_X^\lambda) \log \frac{\text{Dir}(\mathbf{P}_X, \alpha_X^\lambda)}{\text{Dir}(\mathbf{P}_X, \lambda \cdot \mathbf{1})} d\mathbf{P}_X \\ &= \int_{\mathbf{P}_X \in \mathcal{N}_C} \text{Dir}(\mathbf{P}_X, \alpha_X^\lambda) \\ &\quad \log \left(\frac{\Gamma(S_X^\lambda)/\Gamma(C\lambda)}{\prod_{x \in \mathbb{X}} \Gamma(\alpha_X^\lambda(x)) / \Gamma(\lambda)} \prod_{x \in \mathbb{X}} \mathbf{P}_X(x) \alpha_X^\lambda(x)^{-\lambda} \right) d\mathbf{P}_X \\ &= \log \frac{\Gamma(S_X^\lambda)/\Gamma(C\lambda)}{\prod_{x \in \mathbb{X}} \Gamma(\alpha_X^\lambda(x)) / \Gamma(\lambda)} \\ &\quad + \sum_{x \in \mathbb{X}} (\alpha_X^\lambda(x) - \lambda) \int_{\mathbf{P}_X} \text{Dir}(\mathbf{P}_X, \alpha_X^\lambda) \log \mathbf{P}_X(x) d\mathbf{P}_X \\ &= \log \frac{\Gamma(S_X^\lambda)}{\prod_{x \in \mathbb{X}} \Gamma(\alpha_X^\lambda(x))} + \\ &\quad \sum_{x \in \mathbb{X}} (\alpha_X^\lambda(x) - \lambda) (\psi(\alpha_X^\lambda(x)) - \psi(S_X^\lambda)) + K \\ &\approx \log \frac{\Gamma(S_X^\lambda)}{\prod_{x \in \mathbb{X}} \Gamma(\alpha_X^\lambda(x))} + \\ &\quad \sum_{x \in \mathbb{X}} (\alpha_X^\lambda(x) - \lambda) (\psi(\alpha_X^\lambda(x)) - \psi(S_X^\lambda)) \end{aligned} \quad (37)$$

where $\mathbf{1}$ denotes a C -dimensional ones vector, \mathcal{N}_C is a C -dimensional unit simplex, Γ denotes the gamma function, and ψ denotes the digamma function. $\alpha_X^\lambda = \lambda \mathbf{y} + (\mathbf{1} - \mathbf{y}) \odot \alpha_X$ represents a modified Dirichlet parameter vector whose value of the target class has been set to λ instead of 1 in EDL, \odot denotes Hadamard product, and $S_X^\lambda = \sum_{x \in \mathbb{X}} \alpha_X^\lambda(x)$. $K = C \log \Gamma(\lambda) - \Gamma(C\lambda)$ is a scalar which does not affect the optimization result.

A.3 Derivation for Uncertainty Measures

This subsection provides the derivation of several uncertainty measures, including expected entropy, mutual information, and differential entropy, of Dirichlet-based uncertainty models. The following content is adapted from the Appendix of [73] and [29].

Expected Entropy. Let X be a random variable defined in \mathbb{X} , where \mathbb{X} is a domain consisting of multiple mutually disjoint values. Let \mathbf{p} be a probability distribution over \mathbb{X} , and let $\text{Dir}(\mathbf{p}, \alpha)$ be a Dirichlet distribution parameterized by the concentration parameter vector α . If X represents the category index of an input sample, $x \in \mathbb{X} = \{1, \dots, C\}$ denotes the value of X , satisfying $p(X = x) = \mathbf{p}(x)$, then

the expected entropy of the random variable X over the Dirichlet distribution $\text{Dir}(\mathbf{p}, \boldsymbol{\alpha})$ can be derived as follows:

$$\begin{aligned}
 & \mathbb{E}_{\mathbf{p} \sim \text{Dir}(\mathbf{p}, \boldsymbol{\alpha})} [\mathcal{H}[\mathbf{p}(x)]] \\
 &= \int_{\mathbf{p} \in \mathcal{N}_C} \text{Dir}(\mathbf{p}, \boldsymbol{\alpha}) \left(- \sum_{x \in \mathbb{X}} \mathbf{p}(x) \ln \mathbf{p}(x) \right) d\mathbf{p} \\
 &= - \sum_{x \in \mathbb{X}} \int_{\mathbf{p} \in \mathcal{N}_C} \frac{\Gamma(S)}{\prod_{x' \in \mathbb{X}} \Gamma(\boldsymbol{\alpha}(x'))} \\
 & \quad \prod_{x' \in \mathbb{X}} \mathbf{p}(x')^{\boldsymbol{\alpha}(x')-1} (-\mathbf{p}(x) \ln \mathbf{p}(x)) d\mathbf{p} \\
 &= - \sum_{x \in \mathbb{X}} \int_{\mathbf{p} \in \mathcal{N}_C} \frac{\boldsymbol{\alpha}(x)}{S} \frac{\Gamma(S)}{\Gamma(\boldsymbol{\alpha}(x) + 1) \prod_{x' \neq x} \Gamma(\boldsymbol{\alpha}(x'))} \\
 & \quad \prod_{x' \neq x} \mathbf{p}(x')^{\boldsymbol{\alpha}(x')-1} \mathbf{p}(x)^{\boldsymbol{\alpha}(x)} \ln \mathbf{p}(x) d\mathbf{p} \\
 &= - \sum_{x \in \mathbb{X}} \frac{\boldsymbol{\alpha}(x)}{S} \int_{\mathbf{p} \in \mathcal{N}_C} \mathbb{E}_{\mathbf{p} \sim \text{Dir}(\mathbf{p}, \boldsymbol{\alpha} + \mathbf{1}_x)} [\ln \mathbf{p}(x)] d\mathbf{p} \\
 &= - \sum_{x \in \mathbb{X}} \frac{\boldsymbol{\alpha}(x)}{S} (\psi(\boldsymbol{\alpha}(x) + 1) - \psi(S + 1)),
 \end{aligned} \tag{38}$$

where $S = \sum_{x \in \mathbb{X}} \boldsymbol{\alpha}(x)$, \mathcal{N}_C is a C -dimensional unit simplex, ψ denotes the digamma function, and $\mathbf{1}_x$ denotes a one-hot vector with the x -th element being set to 1. The last third equation comes from the property of Gamma function that $\Gamma(n) = (n-1)!$. In some literature, the expected entropy is used to measure the *data uncertainty*.

Mutual Information. In the Dirichlet-based uncertainty methods, the mutual information between the labels \mathbf{y} and the class probability \mathbf{p} , which can be regarded as the difference between the total amount of uncertainty and the data uncertainty, can be approximately computed as:

$$\begin{aligned}
 & \underbrace{I[\mathbf{y}, \mathbf{p}]}_{\text{Distributional Uncertainty}} \\
 & \approx \underbrace{\mathcal{H}[\mathbb{E}_{\mathbf{p} \sim \text{Dir}(\mathbf{p}, \boldsymbol{\alpha})}[\mathbf{p}(x)]]}_{\text{Total Uncertainty}} - \underbrace{\mathbb{E}_{\mathbf{p} \sim \text{Dir}(\mathbf{p}, \boldsymbol{\alpha})}[\mathcal{H}[\mathbf{p}(x)]]}_{\text{Expected Data Uncertainty}} \\
 &= - \sum_{x \in \mathbb{X}} \frac{\boldsymbol{\alpha}(x)}{S} \ln \frac{\boldsymbol{\alpha}(x)}{S} + \sum_{x \in \mathbb{X}} \frac{\boldsymbol{\alpha}(x)}{S} (\psi(\boldsymbol{\alpha}(x) + 1) - \psi(S + 1)) \\
 &= - \sum_{x \in \mathbb{X}} \frac{\boldsymbol{\alpha}(x)}{S} \left(\ln \frac{\boldsymbol{\alpha}(x)}{S} - \psi(\boldsymbol{\alpha}(x) + 1) + \psi(S + 1) \right).
 \end{aligned} \tag{39}$$

The calculation of the expected data uncertainty utilizes the result of Eqn. 38. The mutual information is often used to measure the *distributional uncertainty*.

Differential Entropy. The derivation of the differential entropy of the Dirichlet distribution is given by:

$$\begin{aligned}
 & \mathcal{H}[\text{Dir}(\mathbf{p}, \boldsymbol{\alpha})] \\
 &= - \int_{\mathbf{p} \in \mathcal{N}_C} \text{Dir}(\mathbf{p}, \boldsymbol{\alpha}) \ln \text{Dir}(\mathbf{p}, \boldsymbol{\alpha}) d\mathbf{p} \\
 &= - \int_{\mathbf{p} \in \mathcal{N}_C} \text{Dir}(\mathbf{p}, \boldsymbol{\alpha}) \left(\ln \Gamma(S) - \sum_{x \in \mathbb{X}} \Gamma(\boldsymbol{\alpha}(x)) \right. \\
 & \quad \left. + \sum_{x \in \mathbb{X}} (\boldsymbol{\alpha}(x) - 1) \ln \mathbf{p}(x) \right) d\mathbf{p} \\
 &= \sum_{x \in \mathbb{X}} \ln \Gamma(\boldsymbol{\alpha}(x)) - \ln \Gamma(S) - \sum_{x \in \mathbb{X}} (\boldsymbol{\alpha}(x) - 1) \mathbb{E}_{\mathbf{p} \sim \text{Dir}(\mathbf{p}, \boldsymbol{\alpha})} [\ln \mathbf{p}(x)] \\
 &= \sum_{x \in \mathbb{X}} \ln \Gamma(\boldsymbol{\alpha}(x)) - \ln \Gamma(S) - \sum_{x \in \mathbb{X}} (\boldsymbol{\alpha}(x) - 1) (\psi(\boldsymbol{\alpha}(x)) - \psi(S)).
 \end{aligned} \tag{40}$$

Differential entropy is also a prevalent measure of *distributional uncertainty*. A lower entropy indicates that the model yields a sharper distribution, whereas a higher value signifies a more uniform Dirichlet distribution.

APPENDIX B SUPPLEMENTARY INTRODUCTION

B.1 Uncertainty Reasoning Frameworks

Comparison with Dempster-Shafer Theory (DST) [101]. The DST, often referred to as evidence theory, was initially introduced by Dempster within the realm of statistical inference [102], and Shafer later expanded this theory into a comprehensive framework for representing epistemic uncertainty [101]. DST has been pivotal in shaping subjective logic by challenging the traditional additivity principle of probability theory. Specifically, DST allows the sum of probabilities for all mutually exclusive events to be less than one. This feature enables both DST and subjective logic to explicitly represent uncertainty about probabilities by allocating belief mass to the entire domain. The difference between DST and subjective logic is that, subjective logic encourages the evidence distribution of samples with high uncertainty to fall back onto a prior, while DST does not include a flexible base rate representing the prior distribution.

Comparison with Imprecise Dirichlet Model (IDM) [103]. The IDM for multinomial variables derives upper and lower probabilities by adjusting the minimum and maximum base rates in the Beta/Dirichlet PDF for each possible value within the domain. Unlike subjective logic, which employs a prior weight to influence the base rate's effect, IDM creates an interval of expected probabilities by setting the base rate to its maximum (equal to one) for upper probabilities, and to zero for lower probabilities. It is important to note, however, that the intervals provided by IDM are not strictly bounded, meaning the actual probabilities may fall outside these estimated ranges.

Comparison with Fuzzy Logic [104]. In Fuzzy Logic, variables are defined by terms that have imprecise and partially overlapping meanings. For instance, when considering the variable temperature, potential values might include "Low (0 °C to 20 °C)", "Medium (15 °C to 30 °C)", and "High (25 °C to 40 °C)". Despite the inherent fuzziness of these values, temperature can still be represented in an exact and crisp manner using a *fuzzy membership function*. For example, one could state "The temperature is 0.3 Low and 0.7 Medium", which quantitatively expresses the degree to which the temperature belongs to each vague category. Conversely, in subjective logic, values are inherently crisp, but subjective opinions incorporate an uncertainty mass to capture ambiguity. Fuzzy logic and subjective logic address different aspects of uncertainty, and there is potential to integrate these two approaches by representing fuzzy membership functions using subjective opinions [105].

Comparison with Kleene's Three-Valued Logic [106]. In Kleene's Three-Valued Logic, propositions are categorized as either TRUE, FALSE, or UNKNOWN. A significant limitation of this system is that it broadly labels all non-absolute propositions as UNKNOWN, without providing a detailed quantification of the degree of uncertainty. According to this logic, if two propositions x_1 and x_2 are both classified as

UNKNOWN, their conjunction ($x_1 \wedge x_2$) is also deemed UNKNOWN. This approach leads to a clear issue when dealing with the conjunction of numerous UNKNOWN propositions. Specifically, if n (a sufficiently large number) propositions x_1, x_2, \dots, x_n are all UNKNOWN, their conjunction ($x_1 \wedge x_2 \wedge \dots \wedge x_n$) will also be considered UNKNOWN, even if the probability of the conjunction being TRUE is extremely low. For example, it is reasonable to classify the proposition “the next coin toss will result in heads” as UNKNOWN, but it is counterintuitive to label “the outcome of the next 1,000 coin tosses will all be heads” as UNKNOWN, which should be (almost) FALSE. Subjective logic addresses this paradox effectively. When a series of vacuous opinions are combined, the resulting base rate diminishes towards zero, which in turn minimizes the projected probability. This mechanism ensures that highly unlikely conjunctions are appropriately identified as being close to FALSE.

B.2 Datasets

Following [29], we conduct experiments on the following groups of image classification dataset: (1) **MNIST** [107], **FMNIST** [91], **KMNIST** [92]; (2) **CIFAR-10** [86], **SVHN** [85], **CIFAR-100** [86], **GTSRB** [87], **LFW-People** [88], **Places365** [89], **Food-101** [90]; (3) **mini-ImageNet** [94], **CUB** [95]. Within each group, we designate the first dataset as in-distribution training data, while utilizing the subsequent ones as OOD data. Moreover, to evaluate the effectiveness of our method on video-modality data, we also conduct an open-set action recognition experiment by taking **UCF-101** [96] as ID data and **HMDB-51** [97] and **MiT-v2** [98] as OOD data following [11]. Below are the detailed introductions of the involved datasets:

MNIST [107]. MNIST consists of handwritten digits ranging from 0 to 9. Specifically, MNIST contains 60,000 training images and 10,000 testing images, which have been normalized to fit into 28×28 pixel bounding boxes. We use the proportion of [0.8, 0.2] to partition the training samples into training and validation sets.

FMNIST [91]. FashionMNIST is a dataset designed as a more challenging replacement for MNIST. Created by Zalando Research, FMNIST features grayscale images of various clothing items such as shirts, trousers, sneakers, and bags. The dataset is structured similarly to MNIST, containing 60,000 training images and 10,000 testing images, each of which is 28×28 pixels in size. We use FMNIST as OOD data when training models on MNIST.

KMNIST [92]. Kuzushiji-MNIST is another drop-in replacement for MNIST, consisting of a training set with 60,000 handwritten Kuzushiji (cursive Japanese) Hiragana characters and a testing set comprising 10,000 ones. Similar to MNIST, the handwritten characters have been processed to fit into 28×28 pixel resolution grayscale images. We also use KMNIST as OOD data when using MNIST as ID data.

CIFAR-10 [86]. CIFAR-10 comprises 60,000 32×32 color distributed across 10 distinct classes such as airplanes, birds, cats, ships, and more, with each class containing 6,000 images. Among them, 50,000 are designated for training and the remaining 10,000 for testing. We partition the training images into training and validation sets using a split ratio of [0.95, 0.05].

SVHN [85]. Street View House Numbers dataset consists of digit images of house numbers from Google Street View. Specifically, it contains 73257 digits for training and 26032 digits for testing. We use SVHN as OOD data when training models on CIFAR10.

CIFAR-100 [86]. CIFAR-100 is just like the CIFAR-10, except it has 100 classes containing 600 images each. There are 500 training images and 100 testing images per class. We use CIFAR-100 as OOD data when using CIFAR-10 as ID data.

GTSRB [87]. The German Traffic Sign Recognition Benchmark dataset comprises 43 different traffic sign classes, with a total of 39,209 training images and 12,630 test images. These images are taken under various lighting conditions and environments. In our study, we use the testing set as OOD data when using CIFAR-10 as ID data.

LFWPeople [88]. Labeled Faces in the Wild, a popular face photograph database, contains over 13,000 images of faces collected from the web, each labeled with the name of the person pictured. Of these, 1,680 individuals have two or more distinct photos in the dataset. We use the testing set from the version provided by torchvision as OOD data when using CIFAR-10 as ID data.

Places365 [89]. Places365 includes 1.8 million training images and 36,000 validation images, spanning 365 scene categories. The distribution of images across these categories reflects real-world occurrence frequencies. We use the validation set as OOD data when using CIFAR-10 as ID data.

Food-101 [90]. Food-101 comprises 101 food categories, totaling 101,000 images. Each category includes 250 manually reviewed test images and 750 training images. All images were rescaled to a maximum side length of 512 pixels. We utilize the testing set as OOD data when using CIFAR-10 as ID data.

mini-ImageNet [94]. This database is designed for few-shot learning evaluation. mini-ImageNet comprises 50,000 84×84 color images for training and 10,000 ones for testing, evenly distributed across 100 classes, and these 100 classes are subdivided into sets of 64, 16, and 20 for meta-training, meta-validation, and meta-testing tasks, respectively.

CUB [95]. The Caltech-UCSD Birds dataset contains 11,788 images of 200 subcategories belonging to birds, 5,994 for training and 5,794 for testing. We use CUB as OOD data when using mini-ImageNet as ID data in the few-shot setting.

UCF-101 [96]. UCF-101 is an action recognition data set of realistic action videos, collected from YouTube. Specifically, UCF-101 contains 13320 videos distributed across 101 action categories. For experiments of video-modality setting, we train models on UCF-101 training split and take its testing set as known samples in inference. Following [11], despite there exists a few overlapping classes between UCF-101 and the OOD datasets, HMDB-51 and MiT-v2, we do not manually clean the data for standardizing the evaluation.

HMDB-51 [97]. HMDB-51 is collected mostly from movies, and a small proportion from Prelinger archive, YouTube and Google videos. Specifically, HMDB-51 contains 6,849 clips of 51 action categories, each containing a minimum of 101 clips. We use its testing set as unknown samples in the video-modality setting.

TABLE 13: Comparison of temperature scaling method with EDL-related works in the classical setting, including results evaluated by Expected Calibration Error (ECE) with 15 bins and Brier score. Downward arrows (\downarrow) indicate that lower values correspond to better performance for these metrics.

Method	Confidence Calibration		Mis Detect AUPR	OOD Detect AURP (Mean)
	ECE (15 bins) \downarrow	Brier score \downarrow		
Temp Scale	1.06\pm0.10	18.44 \pm 0.49	98.89 \pm 0.05	82.07 \pm 2.23
EDL	11.56 \pm 0.93	27.34 \pm 0.71	98.74 \pm 0.07	82.32 \pm 0.98
\mathcal{I} -EDL	44.35 \pm 1.27	59.73 \pm 1.31	98.71 \pm 0.11	82.01 \pm 1.47
R-EDL	3.47 \pm 0.31	18.15 \pm 0.50	98.98\pm0.05	83.73 \pm 1.07
Re-EDL	5.72 \pm 0.32	14.95\pm0.47	98.81 \pm 0.05	85.46\pm1.41

MiT-v2 [98]. Multi-Moments in Time has 305 classes and 30,500 testing videos. We also use the testing set as unknown samples for experiments in the video-modality setting.

APPENDIX C

ADDITIONAL EXPERIMENT RESULTS

C.1 Classical Setting

In Table 3 and Table 15, we provide the AUPR and AUROC scores of OOD detection in the classical setting, measured by MP (Max projected probability), UM (Uncertainty Mass), DE (Differential Entropy), and MI (Mutual Information), respectively. Table 13 compares EDL-related works with the temperature scaling method [108] in the classical setting, including results evaluated by the Expected Calibration Error (ECE) with 15 bins and the Brier score. Although temperature scaling achieves impressive results when evaluated by the ECE metric, there still exists a performance gap with our method on OOD detection ability.

Besides, we believe that employing the AUPR scores for evaluation purposes aligns more closely with our objectives than using ECE or Brier score. As delineated in Section 5.3, our primary criterion for assessing uncertainty estimation is the model’s ability in differentiating between ID and OOD samples, as well as between correctly classified and misclassified samples. Despite that ECE is frequently employed to assess the degree of correspondence between the model’s confidence and the true correctness likelihood, a confidence distribution accompanied by a low ECE does not inherently ensure a clear distinction between correct and incorrect predictions. For instance, in a balanced two-class dataset, if a binary classifier categorizes all samples into a single class with a consistent confidence output of 50%, the ECE would be zero, yet this result lacks practical significance.

C.2 Few-shot Setting

Table 16 shows few-shot results of OOD detection measured by more uncertainty metrics, i.e., MP (Max projected probability), UM (Uncertainty Mass), DE (Differential Entropy), and MI (Mutual Information). All results consistently demonstrate the superior OOD detection performance of our proposed method.

C.3 Ablation Study

Due to the space limitation, here we provide the complete versions of Tables 11 and 12 as Tables 17 and 18.

C.4 Visualization of PR and ROC Curves

Figures Fig. 4 and Fig. 5 depict the Precision-Recall (PR) and Receiver Operating Characteristic (ROC) curves, respectively, for differentiating OOD data (SVHN) from ID data (CIFAR-10) using four different uncertainty metrics in a classical setting. Given that we conducted five runs for each method, we selected the run that most closely matched the average performance to plot these curves. As shown in the figures, \mathcal{I} -EDL and R-EDL both outperform the traditional EDL method. Notably, R-EDL exhibits higher precision at low recall levels, indicating that it tends to make more conservative but accurate predictions when detecting OOD samples. Our proposed Re-EDL method, meanwhile, demonstrates the best overall performance.

C.5 Visualization of Uncertainty Distributions

Figs. 6, 7, 8, and 9 show density plots of the normalized uncertainty measures for CIFAR-10 against SVHN, and CIFAR-10 against CIFAR-100. The uncertainty measures include max projected probability, uncertainty mass, differential entropy, and mutual information. We apply min-max normalization on each uncertainty value u , i.e., $u_{\text{norm}} = (u - \min u) / (\max u - \min u)$.

In Fig. 6 and Fig. 7, where max projected probability and uncertainty mass are used as measures of uncertainty, we examine the distributions at the far left of the x-axis for each subplot. The observations indicate that within the EDL, \mathcal{I} -EDL, and R-EDL methods, a prevalent issue is the assignment of nearly zero confidence (or extremely high uncertainty) to a substantial number of ID samples. Consistent with our discussion in Section 4.3, this phenomenon suggests that the adoption of the KL-Div-minimizing regularization excessively suppresses the amplitude of evidence. Consequently, this leads to an overly small total evidence for some ID samples, resulting in excessive uncertainty. In contrast, based on R-EDL, Re-EDL substantially avoids this issue by further deprecating the regularization on non-target evidence, thus achieving a significant performance enhancement. Additionally, in Fig. 8 and Fig. 9, R-EDL and Re-EDL also assign relatively lower uncertainty to ID data and thus exhilarates better separability.

The density plots of \mathcal{I} -EDL show different shapes with other methods, since \mathcal{I} -EDL utilizes the Fisher information matrix to measure the amount of information that the categorical probabilities carry about the concentration parameters of the corresponding Dirichlet distribution, thus allowing a certain class label with higher evidence to have a larger variance. Consequently, the predictions made by the \mathcal{I} -EDL approach are typically less extreme, resulting in a bimodal distribution on the uncertainty density plot where the two peaks are generally closer to the center of the density axis. Moreover, we deduce that the similarity in the shapes of the uncertainty density plots among EDL, R-EDL, and Re-EDL may stem from the fact that our modifications to EDL only consist of relaxations of nonessential settings, without introducing any extra mechanisms.

TABLE 14: List of the hyperparameter λ of experiments in the few-shot setting.

Method	Setting	5-Way 1-Shot	5-Way 5-Shot	5-Way 20-Shot	10-Way 1-Shot	10-Way 5-Shot	10-Way 20-Shot
R-EDL	λ	0.7	0.2	0.3	0.8	0.6	0.7
Re-EDL	λ	0.2	0.1	1.2	0.8	0.3	0.3

TABLE 15: AUROC scores of OOD detection in the classical setting, measured by MP (Max projected probability), UM (Uncertainty Mass), DE (Differential Entropy), and MI (Mutual Information).

Method	CIFAR10 \rightarrow SVHN				CIFAR10 \rightarrow CIFAR100				CIFAR10 \rightarrow GTSRB			
	MP	UM	DE	MI	MP	UM	DE	MI	MP	UM	DE	MI
EDL	84.91 \pm 1.49	84.98 \pm 1.62	84.90 \pm 1.51	84.97 \pm 1.62	84.46 \pm 0.34	84.38 \pm 0.42	84.48 \pm 0.35	84.39 \pm 0.41	83.00 \pm 1.00	82.94 \pm 0.99	83.03 \pm 1.01	82.94 \pm 0.99
\mathcal{I} -EDL	87.44 \pm 1.93	87.22 \pm 1.68	87.49 \pm 1.96	87.24 \pm 1.68	83.95 \pm 0.24	83.82 \pm 0.26	83.99 \pm 0.24	83.83 \pm 0.26	84.04 \pm 1.76	83.73 \pm 1.71	84.04 \pm 1.77	83.75 \pm 1.71
R-EDL	87.47 \pm 1.23	87.47 \pm 1.24	87.54 \pm 0.96	87.47 \pm 1.24	85.26 \pm 0.36	85.26 \pm 0.35	84.90 \pm 0.45	85.26 \pm 0.35	85.50 \pm 0.78	85.50 \pm 0.79	85.24 \pm 0.63	85.50 \pm 0.79
Re-EDL	89.72\pm0.81	92.22\pm1.14	91.79\pm1.08	92.19\pm1.13	85.06\pm0.23	86.67\pm0.14	86.40\pm0.14	86.65\pm0.14	87.42\pm1.55	89.84\pm2.05	89.36\pm1.96	89.80\pm2.04

Method	CIFAR10 \rightarrow LFWPeople				CIFAR10 \rightarrow Places365				CIFAR10 \rightarrow Food101			
	MP	UM	DE	MI	MP	UM	DE	MI	MP	UM	DE	MI
EDL	72.55 \pm 3.56	72.57 \pm 3.69	72.52 \pm 3.57	72.57 \pm 3.69	84.82 \pm 0.53	84.76 \pm 0.67	84.86 \pm 0.56	84.76 \pm 0.66	85.04 \pm 0.60	84.99 \pm 0.59	85.05 \pm 0.60	84.99 \pm 0.59
\mathcal{I} -EDL	73.24 \pm 1.08	73.30 \pm 1.09	73.20 \pm 1.07	73.29 \pm 1.09	84.06 \pm 0.56	83.88 \pm 0.65	84.13 \pm 0.60	83.89 \pm 0.64	84.85 \pm 0.61	84.59 \pm 0.52	84.88 \pm 0.57	84.61 \pm 0.52
R-EDL	75.81\pm2.46	75.81\pm2.46	75.94\pm2.41	75.81\pm2.46	85.79\pm0.55	85.79\pm0.54	85.30\pm0.60	85.79\pm0.54	85.44\pm1.33	85.45\pm1.32	85.20\pm1.38	85.44\pm1.32
Re-EDL	73.63\pm4.29	73.29\pm4.17	73.43\pm4.28	73.31\pm4.19	85.75\pm0.60	87.84\pm0.58	87.45\pm0.59	87.81\pm0.58	85.20\pm0.82	86.56\pm1.04	86.31\pm0.97	86.54\pm1.03

TABLE 16: AUPR scores of OOD detection in the few-shot setting, measured by MP (Max projected probability), UM (Uncertainty Mass), DE (Differential Entropy), and MI (Mutual Information).

Method	5-Way 1-Shot				5-Way 5-Shot				5-Way 20-Shot			
	MP	UM	DE	MI	MP	UM	DE	MI	MP	UM	DE	MI
EDL	66.78 \pm 0.12	65.41 \pm 0.13	69.00 \pm 0.12	66.11 \pm 0.13	74.46 \pm 0.10	76.53 \pm 0.14	77.40 \pm 0.12	76.69 \pm 0.13	80.01 \pm 0.10	79.78 \pm 0.12	80.35 \pm 0.11	79.83 \pm 0.12
\mathcal{I} -EDL	71.79 \pm 0.12	74.76 \pm 0.13	74.04 \pm 0.13	74.70 \pm 0.13	82.04 \pm 0.10	82.48 \pm 0.10	82.30 \pm 0.10	82.47 \pm 0.10	84.29 \pm 0.09	85.40 \pm 0.09	85.12 \pm 0.09	85.35 \pm 0.09
R-EDL	72.91\pm0.12	74.84\pm0.13	74.34\pm0.13	74.76\pm0.13	83.65\pm0.10	84.22\pm0.10	84.05\pm0.10	84.13\pm0.10	84.85\pm0.09	85.57\pm0.09	85.43\pm0.09	85.53\pm0.09
Re-EDL	73.20\pm0.12	75.61\pm0.13	75.65\pm0.13	75.30\pm0.13	83.10\pm0.10	83.35\pm0.10	83.26\pm0.10	83.31\pm0.10	85.19\pm0.09	86.06\pm0.09	85.93\pm0.09	86.06\pm0.09

Method	10-Way 1-Shot				10-Way 5-Shot				10-Way 20-Shot			
	MP	UM	DE	MI	MP	UM	DE	MI	MP	UM	DE	MI
EDL	59.19 \pm 0.09	67.81 \pm 0.12	67.78 \pm 0.12	67.84 \pm 0.12	71.06 \pm 0.10	76.28 \pm 0.10	75.74 \pm 0.10	76.19 \pm 0.10	74.50 \pm 0.08	76.89 \pm 0.09	76.70 \pm 0.08	76.86 \pm 0.09
\mathcal{I} -EDL	71.60 \pm 0.10	71.95 \pm 0.10	71.57 \pm 0.10	71.95 \pm 0.10	80.63 \pm 0.11	82.29 \pm 0.10	81.06 \pm 0.09	81.96 \pm 0.10	81.34 \pm 0.07	82.52 \pm 0.07	82.16 \pm 0.07	82.41 \pm 0.07
R-EDL	72.83\pm0.10	73.08\pm0.10	73.17\pm0.10	73.08\pm0.10	82.39\pm0.09	83.37\pm0.09	82.98\pm0.09	83.28\pm0.09	82.22\pm0.08	82.72\pm0.07	82.48\pm0.08	82.68\pm0.08
Re-EDL	71.48\pm0.10	71.39\pm0.09	70.84\pm0.09	71.38\pm0.09	82.46\pm0.09	83.33\pm0.09	82.87\pm0.08	83.26\pm0.08	82.79\pm0.07	84.09\pm0.07	83.79\pm0.07	84.06\pm0.07

TABLE 17: Validation of the essential EDL setting in the cross entropy (CE) loss formulation by simply replacing softmax classification head with projected probability. Note that this is the complete version of Table 11.

Loss	Method	CIFAR10		\rightarrow SVHN	\rightarrow CIFAR100	\rightarrow GTSRB	\rightarrow LFWPeople	\rightarrow Places365	\rightarrow Food101	Mean
		Cls Acc	Mis Detect	OOD Detect	OOD Detect	OOD Detect	OOD Detect	OOD Detect	OOD Detect	OOD Detect
CE	Softmax	90.11 \pm 0.19	98.91\pm0.06	80.05 \pm 3.04	85.86 \pm 0.67	82.81 \pm 4.17	88.17 \pm 3.32	68.03 \pm 2.72	77.07 \pm 2.26	80.33 \pm 2.70
	Re-EDL	90.48\pm0.25	98.90\pm0.07	85.54\pm1.29	88.65\pm0.37	88.52\pm1.38	89.67\pm1.27	74.42\pm0.67	80.55\pm1.02	84.56\pm1.00
MSE	Softmax	90.10 \pm 0.25	98.87 \pm 0.04	83.62 \pm 3.29	86.54 \pm 0.18	82.77 \pm 2.66	88.22 \pm 2.28	69.57 \pm 2.33	77.09 \pm 3.39	81.30 \pm 2.36
	Re-EDL	90.13\pm0.25	98.81\pm0.05	89.94\pm1.40	88.31\pm0.16	90.53\pm2.04	89.71\pm2.08	73.42\pm1.05	80.83\pm1.72	85.46\pm1.41

TABLE 18: Comparison of common evidence functions. Note that this is the complete version of Table 12.

Evidence Functions	CIFAR10		\rightarrow SVHN	\rightarrow CIFAR100	\rightarrow GTSRB	\rightarrow LFWPeople	\rightarrow Places365	\rightarrow Food101	Mean
	Cls Acc	Mis Detect	OOD Detect	OOD Detect	OOD Detect	OOD Detect	OOD Detect	OOD Detect	OOD Detect
ReLU	83.56 \pm 6.10	98.76 \pm 0.14	84.35 \pm 4.59	85.29 \pm 2.73	85.18 \pm 2.49	88.45 \pm 3.01	68.62 \pm 3.81	78.97 \pm 3.57	81.81 \pm 3.37
Softplus	90.13\pm0.25	98.81\pm0.05	89.94\pm1.40	88.31\pm0.16	90.53\pm2.04	89.71\pm2.08	73.42\pm1.05	80.83\pm1.72	85.46\pm1.41
Exp	89.81 \pm 0.18	98.83\pm0.06	83.72 \pm 2.55	87.16 \pm 0.30	86.43 \pm 2.31	87.80 \pm 3.63	71.72 \pm 1.31	77.50 \pm 2.08	82.39 \pm 2.03

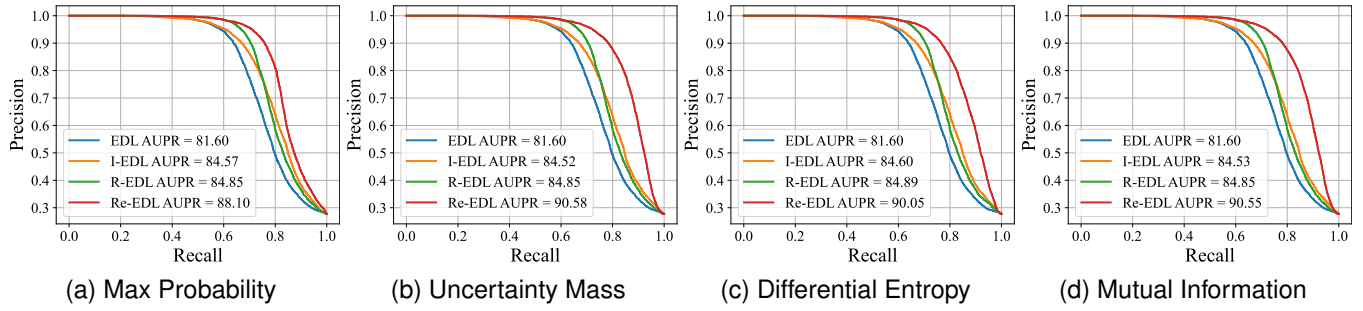


Fig. 4: Precision-Recall (PR) curves of differentiating OOD data (SVHN) from ID data (CIFAR-10).

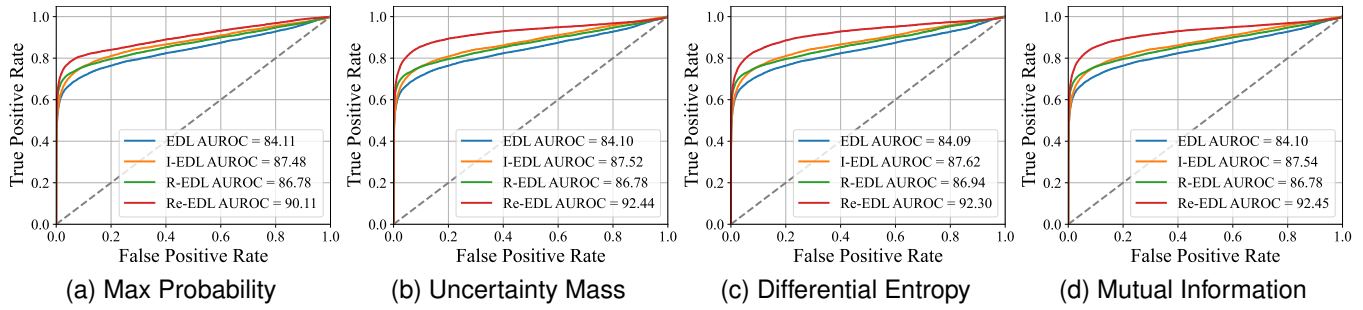


Fig. 5: Receiver Operating Characteristic (ROC) curves of differentiating OOD data (SVHN) from ID data (CIFAR-10).

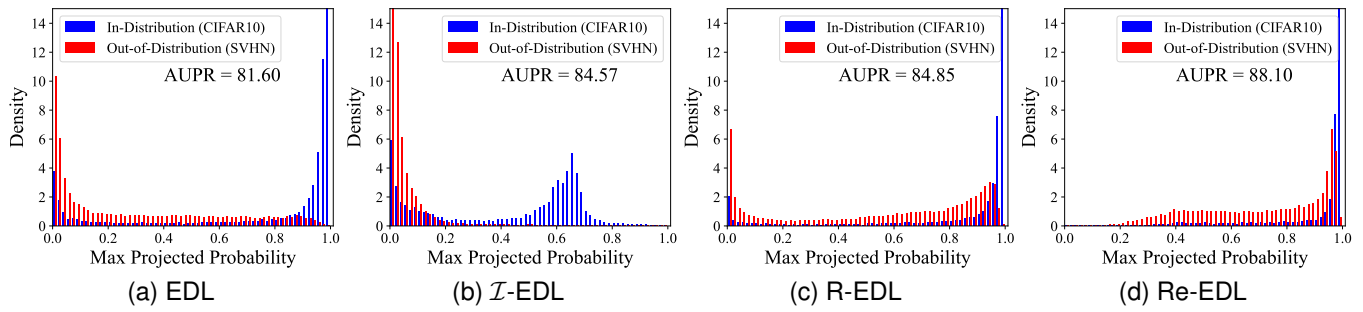


Fig. 6: Uncertainty distribution measured by max projected probability on CIFAR10.

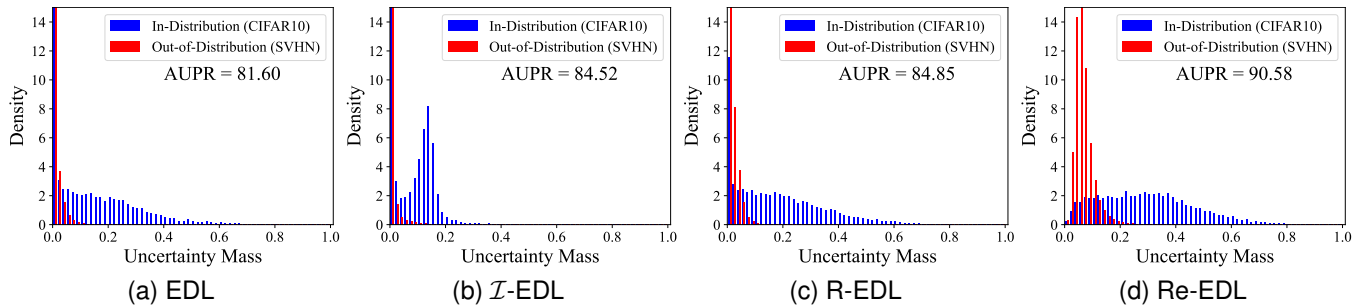


Fig. 7: Uncertainty distribution measured by uncertainty mass on CIFAR10.

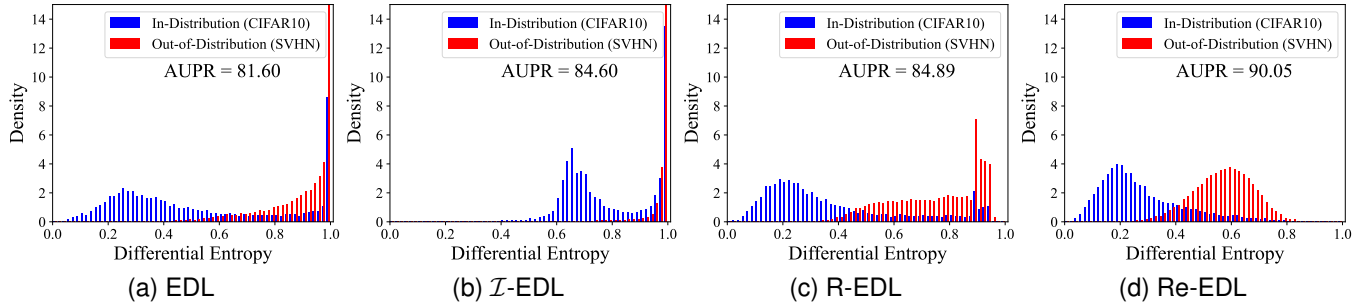


Fig. 8: Uncertainty distribution measured by differential entropy on CIFAR10.

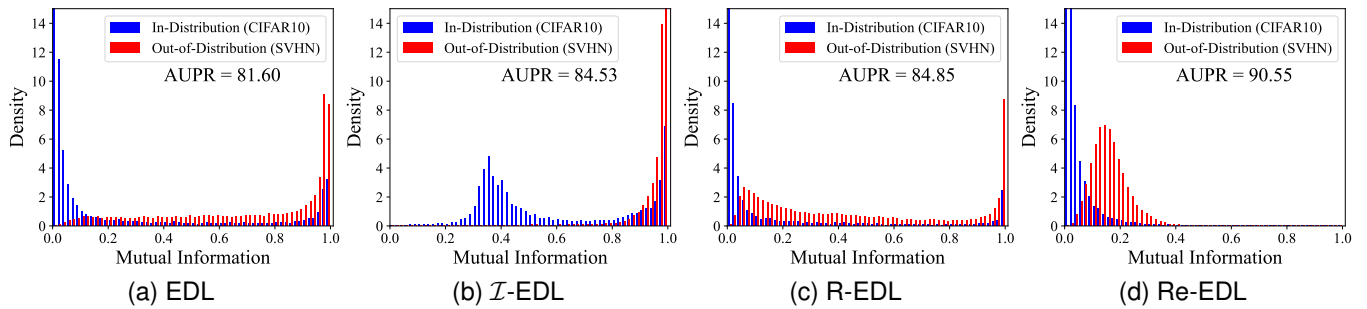


Fig. 9: Uncertainty distribution measured by mutual information on CIFAR10.